From iron to antibiotics: Identification of conserved bacterial-fungal interactions across diverse partners

Emily C. Pierce[1], Manon Morin[1], Jessica C. Little[2], Roland Liu[1], Joanna Tannous[3], Nancy P. Keller[3,4,5], Benjamin E. Wolfe[6], Laura M. Sanchez[2], and Rachel J. Dutton[1,7]

1. Division of Biological Sciences, University of California San Diego, La Jolla, California, USA
2. Department of Medicinal Chemistry and Pharmacognosy, University of Illinois at Chicago, Chicago, Illinois, USA
3. Department of Medical Microbiology & Immunology, University of Wisconsin-Madison, Madison, Wisconsin, USA
4. Department of Bacteriology, University of Wisconsin – Madison, Madison, Wisconsin, USA
5. Food Research Institute, University of Wisconsin – Madison, Madison, Wisconsin, USA
6. Department of Biology, Tufts University, Medford, MA, USA
7. Center for Microbiome Innovation, Jacobs School of Engineering, University of California San Diego, La Jolla, United States

ABSTRACT

Microbial interactions are major determinants in shaping microbiome structure and function. Although fungi are found across diverse microbiomes, the mechanisms through which fungi interact with other species remain largely uncharacterized. In this work, we explore the diversity of ways in which fungi can impact bacteria by characterizing interaction mechanisms across 16 different bacterial-fungal pairs, involving 8 different fungi and 2 bacteria (*Escherichia coli* and *Pseudomonas psychrophila*). Using random barcode transposon-site sequencing (RB-TnSeq), we identified a large number of bacterial genes and pathways important in fungal interaction contexts. Within each interaction, fungal partners elicit both antagonistic and beneficial effects. Using a panel of phylogenetically diverse fungi allowed us to identify interactions that were conserved across all species. Our data show that all fungi modulate the availability of iron and biotin, suggesting that these may represent conserved bacterial-fungal interactions. Several fungi also appear to produce previously uncharacterized antibiotic compounds. Generating a mutant in a master regulator of fungal secondary metabolite production showed that fungal metabolites are key shapers of bacterial fitness profiles during interactions. This work demonstrates a diversity of mechanisms through which fungi are able to interact with bacterial species. In addition to many species-specific effects, there appear to be conserved interaction mechanisms which may be important across microbiomes.

INTRODUCTION

Despite awareness that fungi have an immense capacity to produce biologically active metabolites and to reshape ecosystems, fungi are frequently overlooked in microbiome studies in favor of a bacterial-centric focus[1–3]. Recently, fungi and other microeukaryotes have received increased attention in sequencing-based studies[4–9], and there is growing interest in exploring the role fungi and bacterial-fungal interactions play in environmental and host-associated microbiomes[10–17]. However, the broader patterns and diversity of bacterial-fungal interaction mechanisms have been challenging to characterize given the abiotic and biotic complexity of many microbiomes. While specific interaction mechanisms have been elucidated for particular pairwise bacterial-fungal associations, little is known about the conservation of these

45 mechanisms for other bacterial-fungal pairs and thus about general and widespread interaction
46 mechanisms that could be a major factor in shaping microbiomes.
47 Fermented foods have been developed as experimentally tractable systems to study multi-
48 kingdom microbial communities[18–20]. Cheese rind biofilms, in particular, represent an ideal
49 system to investigate the diversity and conservation of bacterial-fungal interactions due to the
50 presence of culturable bacterial and fungal species representing diverse phyla. Previous work has
51 shown that biofilms that form on the surface of cheese are composed of an average of six
52 bacterial and three fungal genera[18]. These genera are frequently found in natural and human
53 environments, suggesting that interactions in this system may resemble interspecies interactions
54 in other microbiomes. Communities of isolated fungal and bacterial species from cheese can be
55 reassembled in order to investigate how these members interact in coculture[21]. Prior work in this
56 system has demonstrated that fungi in rind biofilms can have both strong positive and negative
57 impacts on bacterial growth and that specialized metabolites can impact these
58 interactions[18,19,22,23].
59 To systematically characterize the potential effects of fungal species on bacteria within
60 this system, we have employed an interdisciplinary approach. Specifically, we used the high-
61 throughput genetic screen RB-TnSeq[24], RNASeq, bacterial cytological profiling, and
62 metabolomics to investigate the diversity of mechanisms through which eight diverse fungal
63 species impact two bacteria (*Escherichia coli* or a cheese-associated *Pseudomonas*
64 *psychrophila*). A previous study used RB-TnSeq in the cheese rind microbiome system to
65 identify interspecies interactions and to characterize the occurrence of higher-order interactions
66 in a microbial community[21]. RB-TnSeq has been used in other systems to identify genes
67 important for host colonization, to determine essential gene sets, and to characterize genes of
68 unknown function[25–27].
69 Here, to infer potential mechanisms of bacterial-fungal interactions, we have developed
70 customized experimental and computational RB-TnSeq pipelines to identify genes impacting
71 bacterial fitness in a mixed biofilm with a fungal partner. We observed a diversity of gene
72 functions that affect bacterial fitness in the presence of a fungal partner. Additionally, we found
73 conservation among the impacts of yeasts and filamentous molds on bacteria; a key example of
74 this is the widespread effect on iron metabolism in bacteria, which is mediated by the acquisition
75 of fungal siderophores. Furthermore, we observed similar effects when we expanded our analysis
76 to include soil and skin fungi, suggesting that this mechanism is relevant not only within cheese
77 rind biofilms, but also in other systems. Consistent with the understanding that fungal species
78 have diverse metabolic repertoires, we find several examples of species-specific effects including
79 the apparent production of antimicrobial compounds by filamentous fungal species. Analysis of a
80 fungal mutant defective in secondary metabolite production revealed changes in the bacterial
81 response compared to the wild type (WT) strain, including genes involved in siderophore uptake
82 and antibiotic resistance. This work provides new perspectives on the biology and mechanisms
83 of bacterial-fungal interactions and highlights the key roles of fungi in microbiomes.

84 **RESULTS**

85 **Selection of Bacterial-Fungal Interaction Partners**

86 To represent fungal diversity within the cheese environment, we selected a panel of 8
87 species of commonly found yeasts and filamentous fungi (Figure 1). The selected fungal species

from cheese rind microbiomes, which represent five different genera and three fungal classes, include two yeasts, *Candida* sp. str. 135E and *Debaryomyces* sp. str. 135B, and filamentous fungi *Penicillium* sp. str. #12*, Penicillium* sp. str. SAM3*, Penicillium* sp. str. RS17*, Fusarium* sp. str. 554A*, Scopulariopsis* sp. str. JB370, and *Scopulariopsis* sp. str. 165-5. These fungal genera were all present at >1% average abundance in 137 geographically diverse cheese microbiomes analyzed in a previous study of rind diversity[18]. These genera are also found in the human gut mycobiome[28], in the soil[29] , and in marine environments[30].

The bacterial interaction partners selected were two species of Gammaproteobacteria, *Pseudomonas psychrophila str.* JB418 and *Escherichia coli*. We decided to focus on Proteobacteria for this work, as they are common inhabitants of cheese rind communities from diverse geographic locations and have been shown to be responsive to the presence of fungi in experimental community conditions[18] (Supplementary Figure 1 and Supplementary Figure 2). *P. psychrophila* is a native and relatively uncharacterized cheese community member isolated from a Robiola due latti cheese rind. *Pseudomonas* species are of interest not only in cheese, but also in human and soil environments[27,31–33]. *E. coli* was also included as a bacterial partner in this study in order to take advantage of the vast genetic resources available for this organism. While *E. coli* is not a common member of cheese rind communities, it is relevant both as a causative agent of foodborne illness in cheese and other foods, and as a commensal member of the human gut microbiome that encounters species from consumed fermented foods[34,35].

Characterization of bacterial genes with differential fitness in the presence of fungal partners

Using a pooled library of barcoded transposon-insertion mutants, RB-TnSeq[24] experiments and analyses generate a fitness value for each gene, reflecting the importance of a gene for survival in the experimental condition. Here, we used RB-TnSeq to identify bacterial mutants that have a differential fitness in the presence of a fungal partner compared to growth alone. To do this, we created a modified experimental and computational pipeline that allowed us to measure and quantitatively compare fitness values across multiple conditions. Previous applications of RB-TnSeq have been designed for intra-condition fitness comparisons, allowing the quantitative comparison of fitness values of different genes within a given condition. However, they were not developed for quantitative inter-condition comparisons, which allow the quantitative comparison of fitness values of the same genes between two different conditions. Specifically, additional normalization steps were needed for inter-condition comparisons. Our updated pipeline includes custom R scripts (available at https://github.com/DuttonLab/RB-TnSeq-Microbial-interactions) which provide step-by-step data visualization to follow the progress of data transformation from raw number of reads to normalized fitness values.

Pooled *P. psychrophila*[21] or *E. coli*[24] RB-TnSeq mutant libraries were grown as a lawn for seven days on solid cheese curd agar (CCA) plates[38] either alone or mixed evenly with one of the eight fungal species (Supplementary Figure 3). Mutant abundances at T0 (inoculation) and day 7 were measured via barcode sequencing and differences in barcode abundance were used to calculate gene fitness values within each condition (Supplementary Data 1 and Supplementary Data 2). To identify genes related to interactions, we looked for mutants whose fitness values were significantly different in a "with fungus" condition versus alone ($p<0.05$) (Figure 2). We hereafter refer to these differences as an interaction fitness. In some cases, the presence of a fungus increases the fitness of a mutant (positive interaction fitness), whereas in others the fitness of a mutant is decreased (negative interaction fitness).

134 In total, we found 453 *E. coli* and 692 *P. psychrophila* genes whose disruption leads to
135 fitness alteration in the presence of at least one of the fungal partners used in this study
136 (Supplementary Data 3 and Supplementary Data 4). This represents an average of 163 ± 24 *E.*
137 *coli* genes per fungal condition and 290 ± 32 *P. psychrophila* genes per fungal condition that
138 have interaction fitness (Figure 3a). These gene sets represent around ten percent of the genes of
139 each bacterium. For *E. coli*, interaction fitness values range from -5.66 to 5.72, and for *P.*
140 *psychrophila,* -6.18 to 6.02. These values are consistent with previously reported fitness values
141 in other experimental systems, where fitness values greater than 2 and less than -2 are generally
142 thought to represent strong fitness effects[24].
143
144 **Comparison of interaction fitness across fungal partners**
145 To assess the specificity of interactions, we evaluated the intersections of gene sets across
146 the entire set of fungal interaction conditions as well as all possible subsets (Figure 3b,
147 Supplementary Data 5 and Supplementary Data 6). A large number of genes show differential
148 fitness only in the presence of specific fungal partners. For *E. coli*, 40 percent of the genes with
149 interaction fitness are specific to a single fungus (n=171), and for *P. psychrophila,* 32 percent
150 (n=219). We identified a number of genes that had interaction fitness across the entire set of
151 partners (n=30 for *E. coli*, and n=65 for *P. psychrophila*). In addition, around 40 percent (n=269)
152 of the interaction-related genes for *P. psychrophila* and 30 percent (n=137) for *E. coli* were
153 common to at least four of the eight fungal interaction conditions. For both *E. coli* and *P.*
154 *psychrophila,* growth with *Penicillium* sp. str. #12 and *Penicillium* sp. str. SAM3 results in a
155 large number of the same genes with significant interaction fitness (Figure 3a and Figure 3b).
156 These species also do not cluster with the other fungi in Principal Component Analysis (PCA) of
157 the raw fitness values for all *E. coli* (left) or *P. psychrophila* (right) genes having interaction
158 fitness in at least one fungal condition (Fig 3c).
159
160 **Mechanisms of fungal impacts on bacterial gene fitness**
161 To identify potential mechanisms underlying bacterial-fungal interactions, we examined
162 the functional distribution of genes associated with interaction fitness. Three functional themes
163 common to multiple fungi used in this study were identified using Clusters of Orthologous Genes
164 (COG) categorization and functional enrichment analysis (Figure 4, Supplementary Data 7 and
165 Supplementary Data 8, Supplementary Figure 4), ranking of strength of fitness effect, and
166 analysis of conservation of the effect across diverse fungal species. These interactions include
167 antimicrobial stress on the bacterial cell envelope, competition for biotin, and provision of
168 bioavailable iron.

169 *Penicillium* sp. str. #12 and *Penicillium* sp. str. SAM3 induce bacterial envelope stress

170 *Penicillium* sp. str. #12 and *Penicillium* sp. str. SAM3 consistently shared impacts on
171 bacterial mutant fitness, as seen by their large number of network connections for both bacteria
172 (Figure 3a and Figure 3b- For *E. coli,* of 116 total genes shared, 22 of these genes are shared
173 only between these two fungi; for *P. psychrophila,* of 187 total genes shared, 19 of these genes
174 are shared only between these two fungi). The genes within this set suggest that these two fungal
175 species are producing antibiotic molecules. For *E. coli*, this overlapping gene set includes the
176 genes encoding for the stress protein CspC, beta-lactam antibiotic resistance membrane protein
177 Blr, and the MdtK multidrug efflux pump. Mutants of these genes displayed decreased fitness in
178 the presence of these fungi. This is also supported by the gene set specific to *Penicillium* sp. str.

179 #12*/E.coli,* which includes a regulator of the EmrA multidrug efflux pump and three gene
180 components of the Rcs regulator of capsule synthesis system (*rcsA, rcsC, rcsD*). The Rcs system
181 can respond to damage to the cell envelope and is induced, for example, by membrane-active
182 antimicrobial peptides[40], peptidoglycan damage caused by inhibition of penicillin-binding
183 proteins[41], and mutations in lipopolysaccharide biosynthesis genes[42]. Additionally, three genes in
184 the *waa* operon (*waaY, waaP, waaQ)* affecting the modification of the heptose region of the core
185 LPS, which plays a crucial role in membrane stability[43], have increased fitness in the presence of
186 *Penicillium* sp. str. #12. WaaY activity is dependent on WaaP and WaaQ[43]. Inactivation of *waaY*
187 has previously been shown to increase *E. coli*'s resistance to antimicrobial peptide LL-37, due to
188 reduced binding of the peptide to the cell surface[44], and it has also been shown to increase
189 resistance of *Salmonella typhimurium* to antimicrobial peptides[45].
190 When grown in coculture with *P. psychrophila,* these two fungi induce an interaction
191 fitness for universal stress protein A, whose mRNA is stabilized by the protein encoded by *cspC,*
192 one of the genes with mutants impacted in *E. coli.* With *Penicillium* sp. str. #12*,* three *P.*
193 *psychrophila* genes involved in LPS/lipid A/outer membrane biogenesis (*msbA, arnB, waaG*)
194 also had interaction fitness. While the *P. psychrophila* genome is not as well documented as *E.*
195 *coli*'s, these data are consistent with the *E. coli* data and with the production of antibiotics by
196 these fungi.
197 To investigate fungal antibiotic activity that could be related to the observed changes in
198 bacterial gene fitness, we modified bacterial cytological profiling (BCP) protocols for use on *in*
199 *vitro* cheese biofilms[46]. This microscopy technique was previously developed to rapidly
200 determine the bacterial cellular pathway targeted by antibiotic compounds. We grew wild type
201 (WT) or Δ*mdtK E. coli* alone or in a mixed biofilm with *Penicillium* sp. str. #12 or *Penicillium*
202 sp. str. SAM3 on CCA plates for seven days. Δ*mdtK E. coli* was chosen due to the RB-TnSeq
203 fitness defect of this mutant specifically in the presence of these *Penicillium.* We performed BCP
204 on bacterial cells either co-cultured in the mixed biofilms or after 2 days of growth on CCA
205 plates with known antibiotic compounds as reference controls (Supp Figure 5, Figure 5).
206 Microscopy showed a strong change in cell morphology for both WT and Δ*mdtK E. coli* when
207 grown with *Penicillium* compared to growth alone (Figure 5). When cultured with these fungi, *E*
208 *coli* cells exhibit a rounded phenotype, consistent with a reduction in cell wall integrity and
209 reminiscent of cells treated with antibiotics that target cell wall biosynthesis such as mecillinam
210 and amoxicillin. Δ*mdtK* cells are strongly affected and have spheroplasted, indicative of the
211 complete loss of structural integrity. Neither of these two fungal strains are known producers of
212 penicillin, and analysis of the draft genomes failed to detect penicillin biosynthesis gene
213 clusters[47]. However, these BCP results are consistent with our RB-TnSeq data and suggest that
214 these two fungal strains are inducing stress on the bacterial cell envelope through an
215 undetermined mechanism that may involve novel antimicrobials.

216 Fungi increase bacterial need for biotin biosynthesis

217 *Pseudomonas* interaction fitness genes suggested competition for environmental biotin
218 between *P. psychrophila* and all of the studied fungal partners. Biotin, found in both milk and
219 cheese,[48] is present in our cheese curd agar medium at 73 nmol/mg and represents an essential
220 cofactor for enzymes involved in key cellular functions like amino acid metabolism and lipid
221 synthesis[49]. Three *P. psychrophila* genes associated with biotin biosynthesis mutants (*bioB,*
222 *bioD, bioF*) have a negative interaction fitness in the presence of all eight fungi. An additional
223 three genes are associated with a negative interaction fitness in the presence of seven fungi

224 (*bioA, bioC, bioH*) (Figure 4). The biotin biosynthesis pathway was significantly enriched in
225 functional enrichment analysis for all fungal partners except *Penicillium* sp. str. SAM3
226 (Supplementary Data 8). Although some species of fungi are capable of biotin biosynthesis,
227 others are capable of only partial synthesis or are incapable [50]. Additionally, differential
228 expression analysis from RNA-Seq of *E. coli* grown either alone or in the presence of
229 *Penicillium* sp. str. #12 showed that *bioA, bioB, bioC, bioD,* and *bioF* were all significantly
230 upregulated in the presence of the fungus with an average fold change of 4.4 (Supplementary
231 Data 9). This highlights an increased need for bacterial biotin synthesis, which again strongly
232 supports that fungi and bacteria are consistently competing for available biotin in the medium.
233 Notably, this interaction appears to be conserved across both bacteria and all fungi.

234 Fungi increase iron availability for bacterial community members

235 Because iron is essential for bacterial growth and cheese is an iron-limited environment,
236 with free iron levels measured to be approximately 3 ppm, microbial species growing on cheese
237 require iron chelators with specific transport systems to sustain their growth[21,51–53]. Our RB-
238 TNseq fitness data revealed that *E. coli* mutants defective in enterobactin transport grow better in
239 the presence of all fungal partners than they do alone (Figure 4, Figure 6a). These genes include
240 members of the *fep* operon (*fepC, fepG, fepA*), which encodes enterobactin transport functions,
241 and *exbD,* which encodes a component of an iron-siderophore transport complex. In the majority
242 of fungal conditions, mutants in an enterobactin esterase encoded by *fes* in addition to iron-
243 siderophore related transport genes *fepB, fepD, tonB* and *exbB* also grow better in the presence of
244 a fungal partner. When grown with any fungal partner, ferric-enterobactin transport is
245 significantly enriched among all the functions associated with genes that have an interaction
246 fitness (Supplementary Data 7).
247 For *P. psychrophila,* we noticed two genes that have a strong fitness defect alone, but
248 positive interaction fitness when any fungus is present. These genes, Ga0212129_114259 (avg.
249 interaction fitness 3.3) and Ga0212129_114260 (avg. interaction fitness 5.3) are annotated as
250 uncharacterized protein DUF3649 and as an uncharacterized iron-regulated membrane protein.
251 The protein encoded by Ga0212129_114259 is 99% identical to an iron transporter from
252 *Pseudomonas fragi* (Acc. WP_133145017.1). Moreover, immediately upstream of these two
253 genes we find a ferric enterobactin receptor (fepA) and the PfeR-PfeS two-component regulatory
254 system required for production of the ferric enterobactin receptor, suggesting that this region
255 may be involved in siderophore uptake. Again, positive interaction fitness for these likely
256 siderophore-uptake associated genes suggests that possibly more iron is available for *P.*
257 *psychrophila* when fungi are present.
258 To validate the RB-TnSeq results related to the Fep system genes, we performed
259 competitive mutant fitness assays with a 1:1 ratio of WT *E. coli* and Δ*fepC,* Δ*fepA,* and Δ*fepG*
260 mutants either alone or in the presence of *Scopulariopsis* sp. str. JB370 or *Penicillium* sp. str.
261 #12. When no fungus is present, there is a clear growth defect for Δ*fep* mutants. After 7 days,
262 both Δ*fepA* and Δ*fepG* mutants grew significantly better with both fungi, whereas there was no
263 difference in wild-type growth with or without fungus. The Δ*fepC* mutant grew significantly
264 better with *Penicillium* sp. str. #12 (Figure 6b).
265 Additionally, differential expression analysis from RNA-Seq of *E. coli* grown on CCA
266 for three days either alone or in the presence of *Penicillium* sp. str. #12 revealed 34 genes (out of
267 a total of 348 significantly upregulated genes) involved in iron acquisition that are specifically
268 upregulated in the presence of the fungus (Supplementary Data 10). Notably, we find genes

269 associated with the uptake machinery for hydroxamate siderophores (including *fhuA* and *fhuE*),
270 which are commonly produced by fungi. We also observe upregulation of enterobactin
271 biosynthesis and uptake, suggesting that *E. coli*, even in the presence of fungi, still produces and
272 utilizes its native siderophore, enterobactin (Figure 6c).
273 All filamentous molds in this study, but not yeast, produce siderophores that were
274 detectable by liquid Chrome Azurol S (CAS) assay (Supplementary Figure 6). Given the positive
275 CAS assays, we next sought to identify the siderophores produced by these fungal species. We
276 performed liquid chromatography mass spectrometry (LC-MS and LC-MS/MS) for all fungal
277 species. This metabolomics data showed evidence of the hydroxamate fungal siderophores
278 coprogen and ferrichrome in *Fusarium* and *Penicillium* species (Figure 6d). Although not
279 detected in these extracts, *Scopulariopsis* sp. str. JB370 is predicted to make dimethylcoprogen
280 based on antiSMASH secondary metabolite biosynthesis gene cluster prediction analysis of the
281 draft genome[54].
282 We hypothesized that the increased fitness of enterobactin *fep* mutants was due to the
283 uptake of fungal siderophores through an alternate pathway. Indeed, we found that coprogen and
284 ferrichrome can rescue the growth defect of Δ*fepA* and Δ*fepC* on CCA (Figure 6e). The *E. coli*
285 Fhu system has previously been shown to allow uptake of hydroxamate-type siderophores[55–58].
286 In *E. coli,* ferrichrome uptake is known to be mediated by the outer membrane receptor FhuA,
287 and coprogen uptake is mediated by the outer membrane receptor FhuE. Mutants of *fhuA* or *fhuE*
288 alone do not show a growth defect on CCA, likely due to the fact that the enterobactin system is
289 intact. Thus, to specifically examine fungal siderophore uptake, we constructed mutants of *fhuA*
290 or *fhuE* in an enterobactin-uptake defective background. Δ*fepA*Δ*fhuA,* Δ*fepA*Δ*fhuE,* and
291 Δ*fepC*Δ*fhuE* were grown on CCA in the presence or absence of fungal siderophores (Figure 6e).
292 Combined loss of enterobactin uptake and *fhuA* eliminates the alleviation seen with ferrichrome,
293 whereas loss of either *fhuA* or *fhuE* in the Δ*fepA* background seems to eliminate the alleviation
294 seen with coprogen. This suggests that *E. coli* requires *fhuA* for ferrichrome uptake, and both
295 *fhuA* and *fhuE* for coprogen uptake.
296 To validate that the fungi used in this study are alleviating *E. coli's* need for enterobactin
297 through the same mechanism, equal volumes of WT or Δ*fep*/Δ*fhu* mutants were spotted on CCA
298 at varying distances from a pre-cultured fungal front (Figure 6f, Supplementary Figure 7).
299 Growth of Δ*fepA* and Δ*fepC* is restored closest to the fungal fronts of all filamentous molds, but
300 not yeast species. For *Penicillium* sp. str. #12, *Scopulariopsis* sp. str. JB370, and *Scopulariopsis*
301 sp. str. 165-5, this effect is lost in the Δ*fepA*Δ*fhuE* and Δ*fepC*Δ*fhuE* double mutant, suggesting it
302 is *fhuE*-dependent. For *Fusarium* sp. str. 554A and *Penicillium* sp. str. RS17*,* it is both *fhuE* and
303 *fhuA*-dependent. For *Penicillium* sp. str. SAM3, loss of *fhuA* decreases but does not totally
304 eliminate alleviation. Thus, we can conclude that in the vicinity of a fungal partner, *E. coli* is
305 likely to use and benefit from fungal hydroxamate siderophores that are taken up by the FhuA
306 and FhuE uptake systems independently of the enterobactin uptake system.
307 Given that iron limitation is a common challenge across many environments, we wanted
308 to examine whether fungal species from other ecosystems could also be producing siderophores
309 accessible to neighboring bacterial species. We performed similar assays with *Aspergillus*
310 *fumigatus,* a soil-dwelling filamentous ascomycete that was originally isolated from the lung
311 tissue of a patient who had aspergillosis[59]. This assay was also performed for *Malassezia*
312 *pachydermatis,* a yeast commensal resident on animal skin. *M. pachydermatis* is also sometimes
313 found on human skin and can act as an opportunistic pathogen; this species has caused
314 bloodstream infections in hospitalized neonates[60,61]. Interestingly, Δ*fepA*Δ*fhuE* and Δ*fepC*Δ*fhuE*

315 mutants are rescued next to *A. fumigatus*, whereas the Δ*fepA*Δ*fhuA* mutant lacking the
316 ferrichrome receptor was not, suggesting that *A. fumigatus* produces a siderophore capable of
317 being imported through FhuA (Figure 6f). *A. fumigatus* is known to produce the extracellular
318 siderophores fusarinine C and triacetylfusarinine C, which are not known to be imported via the
319 Fhu system, and the intracellular siderophore ferricrocin, which is similar to ferrichrome but not
320 expected to be excreted[62]. Ultimately, it is unclear what siderophore is responsible for the effects
321 by *A. fumigatus*. We see a similar effect using *M. pachydermatis,* suggesting that bacteria are
322 able to utilize siderophores from a yeast species using the Fhu system (Figure 6f). *Malassezia*
323 *restricta* and *Malassezia globosa* have previously been found to possess genes for siderophore
324 biosynthesis[63,64]. We performed AntiSMASH[54] analysis on a previously published genome of
325 this *Malassezia pachydermatis* strain, and were able to identify a NRPS biosynthetic gene cluster
326 containing a ferrichrome peptide synthetase[54,65,66]. In sum, our results suggest that diverse fungi
327 can reduce bacterial dependence on their own siderophores by secreting xenosiderophores.

328 **Loss of a fungal secondary metabolite regulator alters the profile of interaction fitness**

329 The cases above show that bacterial gene fitness can be impacted by the production of
330 fungal secondary metabolites, including antimicrobial compounds and siderophores. Previous
331 studies have shown that fungal secondary metabolite production is regulated by the master
332 regulator, LaeA[67]. Loss of LaeA in *Aspergillus* spp., *Fusarium oxysporum,* and *Penicillium*
333 *chrysogenum* is associated with loss of secondary metabolite production[68,69]. To test the impact
334 of alterations in fungal metabolite production on bacterial gene fitness, we generated a Δ*laeA*
335 mutant in *Penicillium* sp. str. #12.
336 To assess the impact of the *laeA* knockout on fungal metabolites in *Penicillium* sp. str.
337 #12, we performed RNA-Seq and liquid chromatography with mass spectrometry (LC-MS) on
338 the WT and *ΔlaeA* mutant. Fourteen percent of the genome (1925 out of 13261 genes) was
339 differentially expressed between WT and *ΔlaeA* (Figure 7a, Supplementary Data 11). This is
340 consistent with previous findings in *A. fumigatus* that LaeA influenced expression of around 10
341 percent of the fungal genome[67]. GO term enrichment analysis identified melanin, organic
342 hydroxy compound, phenol-containing compound, pigment, sterigmatocystin, depsipeptide,
343 lactone, mycotoxin, and organic heteropentacyclic compound biosynthesis as pathways
344 overrepresented in in the set of 1070 genes more expressed in WT (Supplementary Data 12).
345 Among the genes more expressed in WT, we find four genes in a nonribosomal peptide
346 synthetase cluster region predicted by AntiSMASH[54]; these four genes have homology to *sid2,*
347 *sidF, sidH*, and *sitT,* genes associated with siderophore biosynthesis and transport in
348 *Aspergillus*[62]. This gene cluster also includes genes with homology to *sidJ* and *mirB,* providing
349 further evidence that this region has a siderophore-related function. Five genes in a predicted
350 gene cluster encoding production of serinocyclin A and four genes in a predicted cluster
351 encoding production of nidulanin A are also more highly expressed in WT than in *ΔlaeA.* All
352 together, this confirms that deletion of *laeA* is likely to reduce production of fungal secondary
353 metabolites including siderophores. Among the 855 genes more expressed in *ΔlaeA,* GO term
354 enrichment identified amino acid and nucleoside metabolism, fungal cell wall, and ion transport
355 (Supplementary Data 12), highlighting a possible reorganization of *Penicillium* sp. str. #12
356 metabolism in the absence of *laeA*.
357 LC-MS comparison of the two extracts showed differential production of many
358 metabolites, 94 of which have a >10-fold change between the two (Supplementary Data 13). Of
359 these, 93 are less abundant in the *ΔlaeA* mutant, which is consistent with the loss of secondary

360 metabolite production in the *ΔlaeA* mutant (Figure 7b). Some of these metabolites matched with
361 known secondary metabolites and their analogs based on mass and fragmentation pattern.
362 Namely, atlantinone A and cyclopenol were found to be produced by the WT *Penicillium* sp. str.
363 #12 in >10-fold higher quantity than the *ΔlaeA* mutant, and pyripyropene O was putatively
364 identified and produced in >2-fold higher quantity. Cyclopenol is an alkaloid that is described as
365 a mycotoxin in the benzodiazepine class[70] and serves as an biosynthetic intermediate for
366 viridicatol[71], which has been described as having antibacterial activity against *Staphylococcus*
367 *aureus*[72]. Small amounts of viridicatol were indeed found in extracts with high quantities of
368 cyclopenol. Atlantinone A is a meroterpenoid that is derived from the same biosynthetic pathway
369 as other mixed polyketide-terpenoids such as andrastins and citrehybridones produced by various
370 *Penicillium* and *Aspergillus* species[73]. Both pyripyropene O and atlantinone A have tested
371 negative for antimicrobial activity when screened against a panel of bacteria, including an *E. coli*
372 strain[74,75]. The ecological role of these metabolites remains undetermined. In combination with
373 our RNASeq analysis, these data highlight an important diminution of secondary metabolite
374 production in the *ΔlaeA* strain.
375 We next performed RB-TnSeq experiments with the Penicillium sp. str. #12 ΔlaeA
376 mutant to determine whether this single fungal mutation leads to changes in the genes needed for
377 bacterial fitness. While some interaction fitnesses are preserved between ΔlaeA and WT, loss of
378 LaeA appears to significantly change the profile of interactions (Figure 7c). As LaeA is predicted
379 to impact siderophore production, we would expect that E. coli enterobactin uptake mutants
380 would not be as strongly impacted by the presence of the ΔlaeA mutant. Although we see
381 positive interaction fitness of fepA, fepB, fepC and fepG genes when E. coli is grown with WT
382 Penicillium sp. str. #12 relative to E. coli growth alone, we do not see positive interaction fitness
383 of fep genes with ΔlaeA Penicillium sp. str. #12 (Supplementary Data 14). Indeed, liquid CAS
384 assays demonstrate that this mutant produces less siderophores than WT on cheese media (Figure
385 7d). Together, these data support the hypothesis that loss of a fungal secondary metabolite
386 regulator corresponds to changes in bacterial interaction fitness effects.
387 Our RB-TnSeq results, combined with the antibiotic assay BCP, suggested that
388 antibiotic activity by Penicillium sp. str. #12 causes damage to E. coli's cell envelope. As the
389 laeA mutant should have a decreased ability to produce antimicrobial compounds, we examined
390 whether there were changes in the fitness of genes related to responses to antibiotics. The mdtK
391 efflux pump gene, which was previously seen to have negative interaction fitness when grown
392 with WT Penicillium sp. str. #12, no longer has an interaction fitness with ΔlaeA, suggesting that
393 the ΔlaeA mutant has decreased antibiotic production. Although the exact nature of the
394 antimicrobials produced by this strain is unknown, these results are consistent with previous
395 studies, which show that LaeA regulates antibiotic production in other fungal species, and with
396 our metabolite analysis, which showed a decrease in production of many metabolites in ΔlaeA.
397 Overall, these findings suggest that a single fungal gene can strongly impact the bacterial genes
398 needed for fitness and in particular point out that fungal specialized metabolite production may
399 play a large role in determination of bacterial fitness in bacterial-fungal interactions.

400 **DISCUSSION**

401 Fungi have been shown to strongly impact bacterial neighbors in diverse systems, from
402 soil to polymicrobial infections[77–85]. To characterize the effects of fungi from a simple
403 microbiome on bacteria, we used a high-throughput genetic screen, RB-TnSeq, to identify

404 bacterial genes relevant to fungal interactions. We observed a diversity of interactions, in terms
405 of direction (+/-), strength, and mechanism. These mechanisms include effects on important
406 cellular pathways such as biotin synthesis and antibiotic resistance. Our work demonstrates that
407 there is both a large diversity of bacterial-fungal interactions as well as conservation of key
408 interaction mechanisms across different fungi.
409 One of the strongest and most widespread bacterial-fungal interactions that we observed
410 suggests that fungal species can dramatically modulate the access to iron through the provision
411 of fungal siderophores, such as ferrichrome and coprogen. Although it has long been known that
412 bacteria grown in isolation are able to uptake purified fungal siderophores[55,56], our results
413 demonstrate that this exchange takes place between bacteria and fungi growing in a biofilm and
414 that this exchange can have impacts on the competitive fitness of bacteria.
415 Hydroxamate siderophore receptors homologous to FhuE and FhuA are widespread in
416 Proteobacteria, suggesting that this interkingdom siderophore transfer may play an
417 important role in altering metal availability in diverse systems. *Pseudomonas aeruginosa* has
418 previously been shown to produce phenazine metabolites that led to upregulation of extracellular
419 siderophore production by *A. fumigatus*[86]. Fhu uptake systems have also been identified in the
420 Gram-positive bacterial pathogens *Streptococcus agalactiae* and *Listeria monocytogenes*, and
421 growth of non-siderophore producing mutants of *Streptomyces coelicolor* was restored by the
422 presence of siderophores from airborne contaminant fungi[87–90]. Additionally, hydroxamate
423 siderophore uptake systems have been shown to impact *Staphylococcus aureus* fitness in a
424 murine infection model[91]. Another study has shown that the presence of a siderophore-
425 producing, cheese-associated *Scopulariopsis* produced siderophores and caused downregulation
426 of siderophore production by *Staphylococcus equorum*[52]. *Bacteroides fragilis,* a human gut
427 symbiont, is also able to use ferrichrome to grow in iron-limiting conditions, and *fhu* genes are
428 expressed by *E. coli* in colonic mucus[92,93]. Some fungi consumed as a part of fermented foods
429 have been shown to survive digestive system transit, and fermented foods are known to contain
430 fungal siderophores[94,95], which could be a source of fungal siderophores in the gut in addition to
431 potential siderophore production by gut-resident species[94–96]. All together, these results suggest
432 that bacterial use of fungal siderophores may be a widespread mechanism of interkingdom
433 interaction. Considering the crucial role of iron acquisition and metabolism in microbial survival,
434 that this conserved interaction mechanism could be a determinant in shaping environmental and
435 host-associated microbiomes.
436 This study provides new insight into the wide range of fungal impacts on bacteria that
437 can occur even in a simple microbiome. Our data also suggest that even among Proteobacteria,
438 fungal impacts may be diverse. Of the 692 *P. psychrophila* genes and 453 *E. coli* genes that had
439 an interaction fitness with at least one fungal partner, only 58 were homologous based on
440 BLAST (Supplementary Data 15). Further, many genes with interaction fitness do not have a
441 known function. We anticipated that by looking for fungal impacts on *E. coli,* we could leverage
442 the vastly superior genetic information available for this species. However, even in this well-
443 characterized organism, 43% of genes identified as having interaction fitness are annotated as
444 hypothetical or putative. For *P. psychrophila,* 29% of genes with interaction fitness are
445 hypothetical proteins. This highlights that many genes involved in interspecies interactions might
446 yet to be characterized, and that studying microbes in the context of their interactions with other
447 species, and not just in monoculture, provides an avenue for uncovering new areas of biology.
448
449

450 **MATERIALS AND METHODS**

451 Fungal Ribosomal RNA Sequencing

452 Genomic DNA was extracted with phenol-chloroform (pH 8) from cultures of the eight cheese
453 fungal species used in this study. For each extraction: 125 µL of 425–600 µm acid-washed beads
454 and 125 µL of 150–212 µm acid-washed beads were poured in a screw-capped 2 mL tube. 500
455 µL of 2X buffer B (200 mM NaCl, 20 mM EDTA) and 210 µL of SDS 20% were added to the
456 tube as well as the pellet and 500 µL of Phenol:Chloroform (pH 8). Cells were lysed by
457 vortexing the tubes for 2 min at maximum speed. Aqueous and organic phases were separated by
458 centrifugation at 4°C, 8,000 RPM for 3 min and 450 µL of the aqueous phase (upper phase) were
459 recovered in a 1.5 mL eppendorf tube. 45 µL of sodium acetate 3M and 450 µL of ice cold
460 isopropanol were added before incubating the tubes at −80°C for 10 min. The tubes were then
461 centrifuged for 5 min at 4°C at 13,000 RPM. The pellet was then washed in 750 µL of 70% ice
462 cold ethanol and re-suspended in 50 µL of DNAse/RNAse free water. Following DNA
463 extraction, LROR (ACCCGCTGAACTTAAGC) and LR6 (CGCCAGTTCTGCTTACC)[97]
464 primers were used to amplify the large subunit of the ribosomal RNA and for *Penicillium*
465 species, Bt2a (GGTAACCAAATCGGTGCTGCTTTC) Bt2b
466 (ACCCTCAGTGTAGTGACCCTTGGC)[98] primers were used to amplify the beta-tubulin gene.
467 PCR was performed in a final volume of 50 µL: 25 µL of Q5 polymerase master mix (New
468 England Biolab), 2.5 µL of the forward primer at 10 µM, 2.5 µL of the reverse primer at 10 µM,
469 100 ng of genomic DNA, and water using the following PCR programs: LSU-(i) 98°C - 30 s, (ii)
470 35 cycles of: 98°C – 10 s; 52°C – 30 s; 72°C – 1.5 min, (iii) 72°C – 5 min; Beta-tubulin-(i) 98°C
471 - 30 s, (ii) 35 cycles of: 98°C – 10 s; 57°C – 30 s; 72°C – 1 min, (iii) 72°C – 5 min. PCR
472 products were purified with the QIAquick PCR purification kit (Qiagen) and sequenced using the
473 forward and reverse primer by Eton Bioscience Inc (San Diego, USA). Consensus sequences
474 from forward and reverse sequencing reactions were aligned using Geneious version R9 9.1.8
475 (http://www.geneious.com).he MrBayes[36] plugin for Geneious was used to build the
476 phylogenetic tree with the following parameters: Substitution model- JC69; Rate variation-
477 gamma; Outgroup- *Fusarium sp. str. 554A*; Gamma categories-4; Chain Length- 1100000;
478 Subsampling freq- 200; Heated chains-4; Burn-in length- 100000; Heated chain temp- 0.2;
479 Random seed-1160; Unconstrained branch lengths- 1, 0.1, 1, 1.
480

481 Bacterial-Fungal Growth Assays

482 We aimed to inoculate 60000 bacterial cells alone or with 6000 fungal spores per well on 10%
483 cheese curd agar solid medium (CCA medium)[38] adjusted to pH 7 in a 96-well plate. Each
484 bacterial or bacterial-fungal assay was done in triplicate. After 7 days of growth, the entire well
485 was harvested and homogenized in PBS1X-Tween0.05% prior to dilution and plating on LB with
486 20 µg/ml cycloheximide (for bacterial counts) or milk plate count agar with 50 µg/ml
487 chloramphenicol (for fungal spore counts). Counts were done at inoculation and after harvest.
488 Final growth counts were then compared in co-culture condition relative to growth alone to
489 identify interaction impacts. Significant growth impacts were determined based on Dunnett's
490 test[99], p-value < 0.05. Plots were made with R package ggplot2 3.2.1[100].

491 Microbial Culturing for LC-MS/MS extraction

492 All fungal cultures were grown on plate count agar milk salt (PCAMS; 1 g/L whole milk
493 powder, 1 g/L dextrose, 2.5 g/L yeast extract, 5 g/L tryptone, 10 g/L sodium chloride, 15 g/L
494 agar). Plates were kept at room temperature and spores were harvested at 7 days (or until
495 sporulation was observed) of growth for subsequent experiments. Spores harvested from fungi
496 were put into PBS and normalized to an OD_{600} of 0.1 for working stock.

497 Extraction of cultures

498 Three biological replicates of each condition were plated and extracted from solid agar. For
499 extraction from solid agar plates, 5 µL of fungal working stock were spotted onto 10% CCA
500 medium adjusted to pH 7. Following 7 days of growth, agar was removed from the Petri dish and
501 placed into 50 mL falcon tubes. Acetonitrile (10 mL) was added to each tube and all were
502 sonicated for 30 minutes. All falcon tubes were centrifuged and liquid was removed from the
503 solid agar pieces and transferred to 15 mL falcon tubes. The 15 mL falcon tubes containing
504 liquid were then centrifuged and liquid was again removed from any residual solid debris and
505 transferred to glass scintillation vials. These liquid extractions were then dried *in vacuo*. Dried
506 extracts were weighed and diluted with MeOH to obtain 1 mg/mL solutions which were stored at
507 -20°C until analysis via LC-MS/MS.

508 LC-MS/MS data collection

509 High resolution LC-MS and LC-MS/MS data were collected on a Bruker impact II qTOF in
510 positive mode with the detection window set from 50 to 1500 Da, on a 2.1x150mm C18 cortecs
511 UPLC column with a flow rate of 0.5mL/min for a gradient of 10-100% ACN with 0.1% formic
512 acid over 16 minutes. For each sample, 10 μL of a 1mg/mL solution was injected. The ESI
513 conditions were set with the capillary voltage at 4.5 kV. For MS^2, dynamic exclusion was used,
514 and the top nine precursor ions from each MS^1 scan were subjected to collision energies scaled
515 according to mass and charge state for a total of nine data dependent MS^2 events per MS^1. MS^2
516 data for pooled biological replicates is deposited under MassIVE accession number
517 MSV000085070. MS^1 and MS^2 data for *ΔlaeA* and WT *Penicillium sp. str. #12* is deposited
518 under MassIVE accession number MSV000085054 and was collected under identical conditions
519 on a Bruker compact qTOF.

520 Molecular Networking

521 For all extractions, all precursor *m/z*'s that were found in solvent and agar controls (based on
522 both retention time and mass tolerance) were removed prior to input into GNPS using the
523 BLANKA algorithm.[101] A molecular network (
524 https://gnps.ucsd.edu/ProteoSAFe/status.jsp?task=464b331ef9d54de9957d23b4f9b9db14) was
525 created using the online workflow at GNPS. The data was filtered by removing all MS/MS peaks
526 within +/- 17 Da of the precursor m/z. MS/MS spectra were window filtered by choosing only
527 the top 6 peaks in the +/- 50Da window throughout the spectrum. The data was then clustered
528 with MS-Cluster with a parent mass tolerance of .02 Da and a MS/MS fragment ion tolerance of
529 .02 Da to create consensus spectra. Further, consensus spectra that contained less than 2 spectra
530 were discarded. A network was then created where edges were filtered to have a cosine score
531 above 0.7 and more than 6 matched peaks. Further edges between two nodes were kept in the

532 network if and only if each of the nodes appeared in each other's respective top 10 most similar
533 nodes. The spectra in the network were then searched against GNPS' spectral libraries. The
534 library spectra were filtered in the same manner as the input data. All matches kept between
535 network spectra and library spectra were required to have a score above 0.7 and at least 6
536 matched peaks. Solvent and agar control files were also loaded into the networks in order to
537 perform removal based also on fragmentation patterns. All nodes with precursor masses less than
538 200Da were also removed. The extensive background and low *m/z* Da removal was done to more
539 accurately reflect the metabolomic profiles of fungal genera in an attempt to represent only true
540 metabolites. The DEREPLICATOR was used to annotate MS/MS spectra[102,103]. The molecular
541 networks were visualized using Cytoscape software[104].

542 RB-TnSeq Assays

543 All RB-TnSeq assays were performed on 10% CCA medium adjusted to pH 7. Prior to
544 inoculation, one aliquot of each library was thawed and inoculated into 25 mL of liquid LB-
545 kanamycin (50 µg/mL). Once the culture reached mid-log phase (OD = 0.6–0.8), 5 mL of that
546 pre-culture was pelleted and stored at −80°C for the T0 reference in the fitness analysis. The
547 remaining cells were used to inoculate the fitness assay conditions. For each RB-TnSeq fitness
548 assay, we aimed to inoculate seven million cells of the bacterial library (on average 50 cells per
549 insertion mutant). For fitness assays including a fungal partner, 700,000 fungal cells were
550 inoculated based on spore counts. Pre-cultured cells were washed in PBS1X-Tween0.05%,
551 mixed with appropriate volumes of quantified fungal spore stocks, and then inoculated by
552 spreading evenly on a 100 mm petri dish containing 10% CCA medium, pH 7. For each
553 condition, assays were performed in triplicate. After seven days, the plate was flooded with 1.5
554 mL of PBS1X-Tween0.05% and cells were scraped off, taking care to not disturb the CCA. The
555 liquid was then transferred into a 1.5 mL microfuge tube and cells were pelleted by
556 centrifugation. After removing the supernatant, the cells were washed in 1 mL of RNA-protect
557 solution (Qiagen, Hilden, Germany), pelleted and stored at −80°C until gDNA extraction.
558 Genomic DNA was extracted with phenol-chloroform (pH 8) using the same protocol used for
559 fungal gDNA extraction described above. Samples were stored at −80°C until further analysis.
560 After gDNA extraction, extracts containing *Penicillium sp. str. #12* DNA were purified
561 using the OneStep PCR Inhibitor Removal Kit (Zymo Research, CA, USA). Then, the 98°C
562 BarSeq PCR as described in Wetmore et al., 2015 was used to amplify only the barcoded region
563 of the transposons. PCR was performed in a final volume of 50 µL: 25 µL of Q5 polymerase
564 master mix (New England Biolab, MA, USA), 10 µL of GC enhancer buffer (New England
565 Biolab), 2.5 µL of the common reverse primer (BarSeq_P1 – Wetmore et al., 2015) at 10 µM,
566 2.5 µL of a forward primer from the 96 forward primers (BarSeq_P2_ITXXX) at 10 µM and
567 either 200 ng of gDNA for alone conditions, or 2 µg of gDNA for fungal interaction conditions.
568 For *E. coli* analysis, we performed 84 PCRs (T0 sample and 28 harvest samples in triplicate)
569 involving 28 different multiplexing indexes. For *P. psychrophila* JB418 analysis, we performed
570 84 PCRs (T0 sample and 28 harvest samples in triplicate) involving 28 different multiplexing
571 indexes. We used the following PCR program: (i) 98°C - 4 min, (ii) 30 cycles of: 98°C – 30 s;
572 55°C – 30 s; 72°C – 30 s, (iii) 72°C – 5 min. After the PCR, for both *E. coli* and *P. psychrophila,*
573 10 µL of each of the PCR products were pooled together to create the BarSeq sequencing library
574 and 200 µL of the pooled library were purified using the MinElute purification kit (Qiagen,
575 Germany). The final elution of the BarSeq library was performed in 30 µL in DNAse and RNAse
576 free water. The BarSeq libraries were then quantified using Qubit dsDNA HS assay kit

577 (Invitrogen, CA, USA) and sequenced on HiSeq4000 (75 bp, single-end reads), by the IGM
578 Genomics Center at the University of California San Diego. The sequencing depth for each
579 condition varied between 6.1 and 11.7 million reads for *E. coli* and 5.8 and 13.3 million reads for
580 *P. psychrophila.*

581 RB-TnSeq Data Processing

582 Custom R scripts were used to determine the average fitness scores for each gene across three
583 RB-TnSeq assay replicates. These scripts are available at https://github.com/DuttonLab/RB-
584 TnSeq-Microbial-interactions. The Readme document provides an in-depth explanation of all
585 data processing steps performed in these scripts. In brief, insertion mutants that did not have a
586 sufficient T0 count (3) in each condition or that are not centrally inserted (10-90% of gene) were
587 removed from analysis. Counts determined by Wetmore *et al*. scripts were then normalized to a
588 reference gene (*allB* in *E. coli* and closest protein BLAST match Ga0212129_11710 in *P.*
589 *psychrophila*) to be able to compare across conditions and to account for differences in
590 sequencing depth. These genes do not have a strong fitness effect in any condition based on
591 former fitness determination developed by Wetmore *et al.*, 2015. Un-normalized strain fitness
592 was then calculated per insertion mutant as the log2 of the ratio of the corrected counts in the
593 condition and the corrected counts in the T0 sample. Un-normalized gene fitness and variance
594 was next calculated by averaging insertion mutants within a gene. These values were then
595 normalized based on the position of the gene along the chromosome, as well as by the mean of
596 the data distribution. These steps were all done on individual replicates. Next, the average gene
597 fitness and associated variance were calculated using the weighted average of the fitness values
598 across the three different replicates. Then, for each condition, fitness values are corrected by the
599 mean of the replicate means (the replicate means being the mean values used to center fitness
600 value within a replicate). Finally, based on the assumption that most genes should have no fitness
601 effect, we corrected gene fitness values in each condition by the mode (peak of the density
602 distribution). Final fitness values were then compared for fungal interaction conditions compared
603 to bacterial alone conditions and comparisons associated with a p-value lower than 5% were
604 considered significant interaction fitness (alpha parameter=0.05 in
605 2conditions_FitnessComparison.R code). Networks of fitness values were visualized in
606 Cytoscape v. 3.5.1[104] and PCA plots were made with R package ggplot2 3.2.1[100] and ggfortify
607 0.4.7[105]. COG category mapping of *E. coli* and *P. psychrophila* protein sequences was done by
608 eggNOG-mapper[106] and visualized with R package ggplot2 3.2.1[100].

609 Bacterial Cytological Profiling

610 Approximately seven million WT *E. coli* K-12 strain BW25113 or Keio collection *mdtK* mutant
611 cells [107] were inoculated alone or co-inoculated with 700,000 *Penicillium* sp. str. #12 or
612 *Penicillium* sp. str. SAM3 spores on 10% CCA pH 7. After 7 days of growth, 1 mL of T-Base
613 buffer was added to the surface of the biofilms, and biofilms were scraped into the buffer. For
614 co-culture conditions, the sample was filtered through a 0.5 µm filter to specifically remove
615 fungal material. 2 µL of concentrated dye mix (1 µL 1 mg/mL FM4-64, 1 µL 2 mg/mL DAPI in
616 48 µL T-Base) were added to 20 µL of filtrate. Dye-filtrate mix was spotted onto agarose-LB
617 pads (1% Agarose, 20% LB liquid medium, 80% ddH_2O) and imaged by fluorescence and phase
618 contrast. Control compound references on CCA medium were obtained by spotting 30 µL of 5x,
619 10x, 25x, and 100x MIC dilutions of antibiotics onto quadrants on CCA medium pH 7 plates,

620 allowing to dry, and spread-plating 200 µL of log-phase (OD 0.1) *E. coli* cultures. After two
621 days of growth, cells near the edge of the zone of inhibition on appropriate dilution spots were
622 resuspended in 10 µL of prediluted dye mix (1 µL 1 mg/mL FM4-64, 1 µL 2 mg/mL DAPI in
623 998 µL T-Base) and spotted onto agarose-LB pads and imaged as described above. Resulting
624 images were deconvolved using Deltavision SoftWorx software (Applied Precision, Inc., WA,
625 USA), analyzed using Fiji[108], and assembled in Adobe Photoshop (Adobe, CA, USA).

626 CCA medium biotin quantification

627 Biotin quantification of CCA medium was performed on three replicate samples by Creative
628 Proteomics (NY, USA) as follows: 100 mg of each sample was homogenized in water (10
629 µL/mg) for 1 min three times with the aid of 5-mm metal balls on a MM400 mill mixer.
630 Methanol at 10 µL/mg was then added. Water-soluble vitamins were extracted by vortex-mixing
631 for 2 min and sonication in a water batch for 5 min. After centrifugation, the clear supernatants
632 were cleaned up by solid-phase extraction on a Strata-X (60 mg/mL) cartridge. The eluted
633 fractions containing water-soluble vitamins were collected, pooled and then dried under a gentle
634 nitrogen gas flow in a nitrogen evaporator. The residues were dissolved in 200 µL of 10%
635 methanol. Twenty microliter aliquots were injected to run UPLC-MRM/MS with the use of a
636 C18 UPLC column and with (+) ion detection and (-) ion detection, respectively. Calibration
637 curves were prepared by injection of serially-diluted mixed standard solutions of water-soluble
638 vitamins. Concentrations of detected vitamins were calculated by interpolating the linear
639 calibration curves.

640 Δf*ep* mutant competitive growth assays

641 Approximately 600000 WT and Δ*fepA,* Δ*fepC,* or Δ*fepG* Keio collection[107] mutant cells were
642 inoculated at a 1:1 ratio either alone or co-inoculated with approximately 60,000 *Penicillium* sp.
643 str. #12 or *Scopulariopsis* sp. str. JB370 spores on 10% CCA pH 7 in a 96-well plate in four
644 replicates each. After seven days of growth, the entire well was harvested and homogenized in
645 PBS1X-Tween0.05% prior to dilution and plating on LB with 20 µg/ml cycloheximide (total
646 bacterial counts) or with 20 µg/ml cycloheximide and 50 µg/ml kanamycin (bacterial mutant
647 counts). Final growth counts were then compared in co-culture condition relative to growth alone
648 to identify interaction impacts. Significant growth impacts were determined by significantly
649 different growth in the presence of a fungus relative to growth alone based on a two-sample t-test
650 p-value < 0.05. Plots made with R package ggplot2 3.2.1[100].

651

652 RNA-Seq and differential expression analysis of *E. coli* with *Penicillium* sp. str. #12

653 Approximately seven million *E. coli* cells were inoculated in triplicate either alone or with
654 approximately 700,000 *Penicillium* sp. str. #12 spores on 10% CCA pH 7. After 3 days, the
655 biofilms were harvested for RNA extraction and washed with 1 mL of RNAprotect. RNA was
656 extracted by a phenol-chloroform extraction (pH 8) using the same extraction protocol as for
657 gDNA extraction. Extractions were then purified with the OneStep PCR Inhibitor Removal Kit
658 (Zymo Research, CA, USA).
659 Sequencing libraries were prepared as follows. RNA samples were treated with DNAse
660 using the 'Rigorous DNAse treatment' for the Turbo DNA-free kit (AMBION, Life
661 Technologies, Waltham, MA, USA) and RNA concentration was measured by nucleic acid

662 quantification in Epoch Microplate Spectrophotometer (BioTek, Winooski, VT, USA). Transfer
663 RNAs and 5S RNA were then removed using the MEGAclear Kit Purification for Large Scale
664 Transcription Reactions (AMBION, Life Technologies) following manufacturer instructions.
665 Absence of tRNA and 5S RNA was verified by running 100 ng of RNA on a 1.5% agarose gel
666 and RNA concentration was quantified by nucleic acid quantification in Epoch Microplate
667 Spectrophotometer. Also, presence of gDNA was assessed by PCR using universal bacterial 16S
668 PCR primers (Forward primer: AGAGTTTGATCCTGGCTCAG, Reverse Primer:
669 GGTTACCTTGTTACGACTT). The PCR was performed in a final volume of 20 µL: 10 µL of
670 Q5 polymerase master mix (New England Biolabs), 0.5 µL of forward primer 10 uM, 0.5 µL of
671 reverse primer 10 uM and 5 µL of non-diluted RNA. PCR products were run on a 1.7% agarose
672 gel and if gDNA was amplified, another DNAse treatment was performed as well as a new
673 verification of absence of gDNA.
674 Ribosomal RNA depletion was performed using the Ribominus Transcriptome Isolation
675 Kit (Yeast and Bacteria) for the *E. coli* alone samples and using both the Ribominus
676 Transcriptome Isolation Kit (Yeast and Bacteria) and the RiboMinus Eukaryote Kit v2 for the
677 mixed *E. coli/Penicillium sp. str. #12* samples (ThermoFisher Scientific). For the *E. coli* alone
678 samples, each sample was divided into two for treatment and then repooled for RNA recovery
679 with ethanol precipitation. For the *E. coli/*Penicillium sp. str. #12 samples, an equal volume of
680 the eukaryotic probe and RiboMinus Bacterial Probe Mix were used to deplete both bacterial and
681 fungal ribosomal RNA and RNA was recovered with ethanol precipitation. Concentrations after
682 ribosomal RNA depletion were measured using Qubit RNA HS Assay Kits (Invitrogen). The
683 RNASeq library was produced using the NEBNextUltraTM RNA Library Prep Kit for Illumina
684 for purified mRNA or ribosome depleted RNA. We prepared a library with a fragment size of
685 300 nucleotides and used the 10 µM NEBNext Multiplex Oligos for Illumina (Set 1, NEB
686 #E7335) lot 0091412 and the NEBNext multiplex Oligos for Illumina (Set 2, NEB #E7500) lot
687 0071412. We performed PCR product purification with 0.8X Agencourt AMPure XP Beads.
688 Library samples were quantified with Qubit DNA HS Assay Kits before the quality and fragment
689 size were validated by TapeStation (HiSensD1000 ScreenTape). Library samples were pooled at
690 a concentration of 15 nM each and were sequenced on HiSeq4000 (50 bp, single-end).
691 TapeStation assays and sequencing were performed by the IGM Genomics Center at the
692 University of California San Diego.
693 Following sequencing, reads were mapped to the concatenated genome of *E. coli* K12
694 BW25113[109] and *Penicillium* sp. str. #12 using Geneious version R9 9.1.8
695 (http://www.geneious.com). Only the reads that uniquely mapped to a single location on the *E.*
696 *coli* genome section were kept. *E. coli* expression analysis was performed using the following R
697 packages: Rsamtools (R package version 2.0.3), GenomeInfoDb (R package version 1.20.0),
698 GenomicFeatures[110] (R package version 1.36.4), GenomicAlignments[110] (R package version
699 1.20.1), GenomicRanges[110] (R package version 1.36.1) and DESeq2[111] (R package version
700 1.20.1). We followed the workflow described by Love et al. and performed the differential
701 expression analysis using the package DESeq2. Differentially expressed genes between two
702 conditions were selected with an adjusted p-value lower than 5% (Benjamini-Hochberg
703 correction for multiple testing) and an absolute log2 of fold change equal to or greater than 1.5.

704 Construction of *E. coli* mutants and visual interaction assays

705 Visual assays for hydroxamate siderophore stimulation:

706 Antibiotic assay discs (Whatman) were placed on CCA medium pH 7 with .005% tetrazolium
707 chloride (an indicator of cellular respiration) and 20 µl of water, 10 µM coprogen or ferrichrome
708 (EMC Microcollections GmbH) solutions (in water) were slowly pipetted onto the disc and
709 allowed to absorb. 2.5 µl of *E. coli* 37°C overnight LB cultures of *E. coli* K12 BW25113 WT,
710 Δ*fepA,* Δ*fepC,* Δ*fhuE,* Δ*fhuA,* Δ*fepA*Δ*fhuE,* Δ*fepC*Δ*fhuE,* or Δ*fepA*Δ*fhuA* mutants[107] and were
711 spotted next to the discs. Double mutants were constructed as described below. Plates were left
712 at room temperature until red color developed.

713 Visual assays for fungal stimulation of bacterial mutants:

714 Fungal spores were inoculated on CCA pH 7 with .005% tetrazolium chloride. After a week of
715 fungal growth at room temperature (cheese fungal isolates) or 30°C (gut yeast) , 2.5 µl of *E. coli*
716 37°C overnight LB cultures were spotted at increasing distances from the fungal front. Plates
717 were left at room temperature until red color developed. *A. fumigatus* isolate AF293 was
718 received from Nancy Keller, University of Wisconsin-Madison. *M. pachydermatis* was originally
719 isolated from the ear of a dog in Sweden (ATCC14522).

720 Creation of Δ*fepA*Δ*fhuE* and Δ*fepC*Δ*fhuE*:

721 Chemically competent cells for Δ*fepA* or Δ*fepC* mutants were created. An overnight culture of
722 Δ*fepA* or Δ*fepC* mutants was diluted 1:100 and grown at 37°C until OD 0.4-0.6. The culture was
723 placed on ice for 20 minutes and then centrifuged at 4°C for 10 minutes at 6000 rpm to collect
724 the cells. Supernatant was removed and cells were resuspended in half the previous volume of
725 pre-cooled 0.1M CaCl2. After being left on ice for 30 minutes, centrifugation was repeated and
726 supernatant was removed before resuspension in a quarter of the original volume of pre-cooled
727 0.1M CaCl2/15% glycerol. Cells were aliquoted and stored at -80°C until transformation. These
728 cells were transformed with the pKD46 plasmid [112], recovered at 30°C and plated on LB plates
729 with 100 µg/mL Ampicillin and grown at 30°C. Overnight cultures were started from individual
730 colonies for creation of electrocompetent cells. Overnight cultures of Δ*fepC*-pkD46 or Δ*fepA*-
731 pkD46 were diluted 1:100 in fresh LB- 100 µg/mL Ampicillin and grown at 30°C until an OD of
732 0.1. 20 ul of fresh 1 M L-arabinose were added and growth was continued at 30°C until OD 0.4-
733 0.6. Cells were then chilled on ice for 15 minutes and then centrifuged for ten minutes at 4000
734 rcf 4°C. Cells were resuspended in 1 mL of ice water and centrifuged for ten minutes at 4000 rcf
735 at 4°C. Cells were resuspended in 0.5 mL of ice water and centrifuged for ten minutes at 4000 rcf
736 4°C. Cells were resuspended in 50 uL of ice water and kept on ice until transformation. The
737 chloramphenicol resistance cassette was amplified from the pKD3 plasmid [112] using the custom
738 primers: FhuEcatF
739 (CAGATGGCTGCCTTTTTTACAGGTGTTATTCAGAATTGATACGTGCCGGTAATGGCG
740 CGCCTTACGCCCC) and FhuEcatR
741 (CCTCCTCCGGCATGAGCCTGACGACAACATAAACCAAGAGATTTCAAATGCTGGGC
742 CAACTTTTGGCGAA) and the following PCR conditions (i) 98°C - 30 sec, (ii) 30 cycles of:
743 98°C – 10 s; 70°C – 20 s; 72°C – 30 s, (iii) 72°C – 5 min. Amplification was performed on 4 ng
744 of pKD3 plasmid using Q5 High-Fidelity 2X Master Mix (New England Bioloab). The PCR
745 product was digested for 1 hour with the restriction enzymes DpnI and ClaI at 37°C and then the
746 PCR product was run on a 1% agarose gel. The PCR product was extracted using the QIAquick
747 Gel Extraction Kit (Qiagen) and then dialyzed for 4 hours with TE buffer. 1.5 ul of dialyzed PCR
748 product was used to transform the electrocompetent Δ*fepC*-pkD46 or Δ*fepA*-pkD46 cells. After
749 2 hours of recovery in SOC medium with 1mM arabinose at 37°C, the transformation was plated
750 on LB with 50 µg/mL kanamycin and chloramphenicol. Transformants were confirmed to be

751 Δ*fhuE* with Eton Bioscience Inc. sequencing of the chloramphenicol cassette.

752 Creation of Δ*fepA*Δ*fhuA:*

753 Creation was done as with Δ*fepA*Δ*fhuE,* except that the chloramphenicol resistance cassette was
754 amplified from pKD3 [112] using FhuAcatF (ATCATTCTCGTTTACGTTATCATTCACTTT
755 ACATCAGAGATATACCAATGAATGGCGCGCCTTACGCCCCAATGGCGCGCCTTACG
756 CCCC) and FhuAcatR
757 (GCACGGAAATCCGTGCCCCAAAAGAGAAATTAGAAACGGAAGGTTGCGGTCTGGG
758 CCAACTTTTGGCGAACTGGGCCAACTTTTGGCGAA) custom primers.

759 *Penicillium* sp. str. #12 genome sequencing, assembly, and annotation

760 Genomic DNA was extracted from *Penicillium* sp. str. #12 using the genomic DNA extraction
761 protocol described above. High molecular weight DNA (average 16 Kb) was sequenced on the
762 Oxford Nanopore MinION with a R.9.5 flow cell using $1D^2$ sequencing adaptors from kit SQK-
763 LSK308 (Oxford Nanopore Technologies, Oxford, United Kingdom). Raw data was basecalled
764 using guppy 3.3.0 (Oxford Nanopore Technologies, Oxford, United Kingdom)(guppy_basecaller
765 -config dna_r9.5_450bps.cfg --fast5_out) for 1D basecalls and these were used to also obtain
766 higher accuracy 1D^2 basecalls (guppy_basecaller_1d2 -i 1Dbasecall/workspace/ --config
767 dba_r9.5_450bps_1d2_raw.cfg --index_file 1Dbasecall/sequencing_summary.txt) These reads
768 were assembled by canu 1.8[113] and polished by racon 1.4.3[114] four times and by pilon 1.23[115]
769 once. The final assembly is 38 Mbp and consists of 52 contigs.

770 Then, *Penicillium* sp. str. #12 genome annotations were obtained by combining genomic and
771 transcriptomic information from RNASeq. To obtain the gene expression profile of *Penicillium*
772 sp. str. #12, approximately 700,000 WT *Penicillium* sp. str. #12 spores were inoculated in
773 triplicate on 10% CCA pH 7. After 3 days, the biofilms were harvested for RNA extraction and
774 washed with 1mL of RNAprotect. RNA was extracted and RNA-Seq libraries were prepared as
775 described above with the following modification: Ribosomal RNA depletion was performed
776 using the RiboMinus Eukaryote Kit v1 and RNA was recovered with ethanol precipitation. After
777 sequencing, the RNASeq reads from these *Penicillium* sp. str. #12 alone cultures were
778 concatenated with RNASeq reads from the previously described *E. coli/Penicillium* sp. str. #12
779 coculture conditions that uniquely mapped to a single location on the *Penicillium* sp. str. #12
780 genome. The full set of transcriptomic reads were then used as input into the FunGAP annotation
781 pipeline and 77 million of these reads mapped[116]. This pipeline predicted 13261 protein-coding
782 genes in the *Penicillium* sp. str. #12 genome. Interproscan[117] was used within the FunGAP
783 pipeline for function prediction of genes.

784 Creation and confirmation of *laeA* deletion in *Penicillium* sp. str. #12

785

786 *Deletion cassette design strategy:* In order to knockout *laeA* in *Penicillium* sp. str. #12, the
787 isolate was first screened for hygromycin and phleomycin resistance, two antibiotics that are
788 commonly employed by our group as selectable markers. *Penicillium* sp. str. #12 showed a
789 confirmed sensitivity to both antibiotics. A three round PCR deletion strategy was used to
790 replace the *laeA* ORF with the *hph* gene, whose expression confers selection on hygromycin[118].
791 The schematic representation of the *laeA* gene replacement with the hph gene is depicted in
792 Supplementary Figure 8. The deletion cassette (5'flank- hph- 3'flank) was constructed using

793 three sequential PCR reactions. In the first PCR round, about 1kb genomic sequence that flank
794 either the 5' or 3' end of the *laeA* ORF were amplified from strains 12 using respectively the
795 primer sets P12_KOlaeA_5' F (CTCCGTTGGGCCCTCAC) and 5'R
796 (GCAATTTAACTGTGATAAACTACCGCATTAAAGCTGTTGATATCGGCAATCAATCA
797 ATG) or P12_KOlaeA_3'F
798 (GGTGGGCCTTGACATGTGCAGCCGGTGGAGCGGCGCCTGGTGAATCCTACCCACAT
799 GG) and 3'R (CGTTGGGAGGAAAAGCTTCTGCG). The *hph* gene was amplified from
800 plasmid pUCH2-8 using primers hph_F (AGCTTTAATGCGGTAGTTTATCACAG) and hph_R
801 (CTCCACCGGCTGCACATGTC). A second PCR reaction was performed to assemble by
802 homologous recombination the three individual fragments from the first round PCR. The
803 deletion cassettes were finally amplified using the nested primer set, P12_KOlaeA_NestedF
804 (CAGACGGTCCGCATCCCG) and P12_KOlaeA_NestedR
805 (GGTCCAGGTGCAGTAGTACTG).
806
807 *Fungal transformation:* To generate the deletion strains, a protoplast-mediated transformation
808 protocol routinely used by our group was employed and improved to achieve a successful
809 protoplasting of these *Penicillium* sp. strains. Briefly, 109 fresh spores from each strain are
810 cultured in 500 mL of LMM for 12 h under 25 °C and 280 rpm. Newly born hyphae were
811 harvested by centrifugation at 8000 rpm for 15 min and hydrolyzed in a mixture of 30 mg Lysing
812 Enzyme from Trichoderma (Sigma-Aldrich) and 20 mg Yatalase (Fisher Scientific) in 10 mL of
813 Osmotic Medium. The quality of protoplast was monitored under the microscope after four hours
814 of shaking under 28 °C and 80 rpm. The protoplast mixture was later overlaid with 10 mL of
815 trapping buffer and centrifuged for 15 min under 4 oC and 5000 rpm. Protoplast were collected
816 from the interface, overlaid with an equal volume of STC (1M sorbitol, 10 mM Tris-HCL and 10
817 mM CaCl2) and decanted by centrifugation at 6000 rpm for 8 min. The protoplast pellet was
818 resuspended in 500 µL STC and used for transformation.
819 After 5 days of incubation at 25 °C, colonies grown on SMM plates supplemented with
820 hygromycin were subjected to a second round of selection on hygromycin plates. In total, 25
821 hygromycin-resistant transformants were isolated after a rapid screening procedure on SMM
822 supplemented with hygromycin. Single-spored transformants were later tested for proper
823 homologous recombination at the ORF locus by PCR and Southern blot analysis.
824
825 *Gene-deletion strain confirmation:* The correct replacement of the *laeA* with the *hph* gene was
826 first verified by PCR analysis of genomic DNA derived from the transformant strains using
827 primer set P12_laeA_F (CACAATGGCTGAACACTCTCGG) and P12_laeA_R
828 (GGGATATGGAGCATCGAAGTTGC), that amplify the *laeA* ORF. About 12% (3/25) of the
829 monoconidial lines generated from primary transformants of stains 12 were PCR-positive for the
830 absence of the *laeA* ORF. The positive deletion strains were further checked for a single insertion
831 of the deletion cassette by Southern blot analysis and revealed single-site integration of the
832 deletion cassette in one transformant (Supplementary Figure 8). Probes corresponding to the 5'
833 and 3' flanks of the *laeA* gene in each strain were labeled using [α32P] dCTP (PerkinElmer,
834 USA) following the manufacturer's instructions.
835
836 RNA-Seq analysis of WT and Δ*laeA Penicillium sp. str. #12*

837 To characterize the effect of the *laeA* deletion on the *Penicillium* sp. str. #12 gene expression
838 profile, we performed RNA-Seq analysis for Δ*laeA Penicillium* sp. str. #12. As for WT

839 *Penicillium* sp. str. #12, 700,000 Δ*laeA Penicillium* sp. str. #12 spores were inoculated in
840 triplicate on 10% CCA pH 7 and biofilms were harvested after 3 days. Harvest, RNA extraction
841 and library preparation were performed identically to WT *Penicillium* sp. str. #12. Then,
842 *Penicillium* sp. str. #12 and Δ*laeA* differential expression analysis was performed as described
843 for *E. coli/Penicillium* sp. str. #12 above. To look for enrichment of functions in the set of
844 differentially expressed genes, we input the protein sequences of the genes into the gene-list
845 enrichment function of KOBAS 3.0[119]. Sequences were searched against the Gene Ontology
846 (GO) database[120,121] using *A. fumigatus* as a reference for GO assignment before conducting a
847 hypergeometric test with Benjamini-Hochberg correction. Functions with a corrected p-value
848 <.05 were considered enriched.

849

Reagent type (species) or resource	Designation	Source or reference	Identifiers	Additional information
Library, strain background (*Escherichia coli* K12)	Keio collection	PMID: 16738554	CGSC, RRID:SCR_002303	Collection of 3,818 *E. coli* knockout strains
Library, strain background (Escherichia coli K12)	Keio_ML9	PMID: 25968644		RB-TnSeq library of *E. coli* K12 BW25113 (152,018 pooled insertion mutants)
Library, strain background (*Pseudomonas psychrophila*)	JB418_ECP1	PMID: 30211673		RB-TnSeq library generated in the *P. psychrophila* JB418 strain isolated from cheese (272,329 pooled insertion mutants)
Strain, strain background (*Escherichia coli* K12)	Keio ME9062	PMID: 16738554	CGSC#: 7636	Parent strain of the Keio collection mutants
Penicillium sp. str. SAM3		Danisco - CHOOZIT	PC SAM 3 LYO 10D	Industrial starter for cheese production
P. psychrophila	*Pseudomonas psychrophila* JB418	PMID: 30211673		Strain isolated from Robiola due latti cheese
Candida sp. str. 135E		This paper		Strain isolated from chees
Debaryomyces sp. str. 135B		This paper		Strain isolated from cheese
Penicillium sp. str. #12		This paper		Strain isolated from cheese
Penicillium sp. str. RS17		This paper		Strain isolated from cheese
Scopulariopsis sp. str. JB370.		This paper		Strain isolated from cheese

Scopulariopsis sp. str. 165-5		This paper		Strain isolated from cheese
Fusarium sp. str. 554A		This paper		Strain isolated from cheese
Aspergillus fumigatus	*A. fumigatus* str. AF293	Nancy Keller, University of Wisconsin-Madison		
Malassezia pachydermatis	*M. pachydermatis* str. CBS 1879	ATCC14522		

ACKNOWLEDGMENTS

The authors would like to thank: the Arkin lab and the Deutschbauer lab at UC-Berkeley for the *E. coli* Keio_ML9 library, Kristen Jepsen at the IGM Genomics Center at the University of California San Diego for assistance with sequencing, Dr. Sergey Kryazhimskiy (UCSD) for his input on RB-TnSeq data processing, Cong Dinh (UCSD) for assistance with fungal genome assembly, William Bushnell for assistance with fitness validation experiments, Dr. Sinem Beyhan for advice on fungal genome annotation, Drs. Joe and Kit Pogliano (UCSD) for the use of their microscope, Lisa Marotz (UCSD) for assistance with non-cheese yeasts, and members of the Dutton lab, especially Brooke Anderson, for constructive comments on the manuscript.

FUNDING SOURCES

This work was supported by NSF grant MCB-1817887: Chemical and genetic mechanisms driving microbial interactions in a model microbiome (R.D. and L.S.), the UCSD Center for Microbiome Innovation (E.P.), the UCSD Ruth Stern Award (E.P.), NIH Institutional Training grant 5 T32 GM 7240-40 (E.P.), and NIH R01GM112739-01 (N.P.K.).

REFERENCES

1. Laforest-Lapointe, I. & Arrieta, M.-C. Microbial Eukaryotes: a Missing Link in Gut Microbiome Studies. *mSystems* **3**, (2018).
2. Forbes, J. D., Bernstein, C. N., Tremlett, H., Van Domselaar, G. & Knox, N. C. A Fungal World: Could the Gut Mycobiome Be Involved in Neurological Disease? *Front. Microbiol.* **9**, 3249 (2018).

872 3. Huseyin, C. E., O'Toole, P. W., Cotter, P. D. & Scanlan, P. D. Forgotten fungi-the gut
873 mycobiome in human health and disease. *FEMS Microbiol. Rev.* **41**, 479–511 (2017).
874 4. Bergelson, J., Mittelstrass, J. & Horton, M. W. Characterizing both bacteria and fungi
875 improves understanding of the Arabidopsis root microbiome. *Sci. Rep.* **9**, 24 (2019).
876 5. Huffnagle, G. B. & Noverr, M. C. The emerging world of the fungal microbiome. *Trends*
877 *Microbiol.* **21**, 334–341 (2013).
878 6. Soverini, M. *et al.* HumanMycobiomeScan: a new bioinformatics tool for the
879 characterization of the fungal fraction in metagenomic samples. *BMC Genomics* **20**, 496
880 (2019).
881 7. Bradford, L. L. & Ravel, J. The vaginal mycobiome: A contemporary perspective on fungi
882 in women's health and diseases. *Virulence* **8**, 342–351 (2017).
883 8. Marsh, A. J., O'Sullivan, O., Hill, C., Ross, R. P. & Cotter, P. D. Sequence-based analysis
884 of the bacterial and fungal compositions of multiple kombucha (tea fungus) samples. *Food*
885 *Microbiol.* **38**, 171–178 (2014).
886 9. De Filippis, F., Laiola, M., Blaiotta, G. & Ercolini, D. Different Amplicon Targets for
887 Sequencing-Based Studies of Fungal Diversity. *Appl. Environ. Microbiol.* **83**, (2017).
888 10. Fan, D. *et al.* Activation of HIF-1α and LL-37 by commensal bacteria inhibits Candida
889 albicans colonization. *Nat. Med.* **21**, 808–814 (2015).
890 11. Jiang, T. T. *et al.* Commensal Fungi Recapitulate the Protective Benefits of Intestinal
891 Bacteria. *Cell Host Microbe* **22**, 809–816.e4 (2017).
892 12. Wheeler, M. L. *et al.* Immunological Consequences of Intestinal Fungal Dysbiosis. *Cell*
893 *Host Microbe* **19**, 865–873 (2016).
894 13. Peleg, A. Y., Hogan, D. A. & Mylonakis, E. Medically important bacterial–fungal

895 interactions. *Nat. Rev. Microbiol.* **8**, 340–349 (2010).

896 14. Mason, K. L. *et al.* Interplay between the gastric bacterial microbiota and Candida albicans
897 during postantibiotic recolonization and gastritis. *Infect. Immun.* **80**, 150–158 (2012).

898 15. Wagg, C., Schlaeppi, K., Banerjee, S., Kuramae, E. E. & van der Heijden, M. G. A. Fungal-
899 bacterial diversity and microbiome complexity predict ecosystem functioning. *Nat.*
900 *Commun.* **10**, 4841 (2019).

901 16. Durán, P. *et al.* Microbial Interkingdom Interactions in Roots Promote Arabidopsis Survival.
902 *Cell* **175**, 973–983.e14 (2018).

903 17. Tourneroche, A. *et al.* Bacterial–Fungal Interactions in the Kelp Endomicrobiota Drive
904 Autoinducer-2 Quorum Sensing. *Frontiers in Microbiology* vol. 10 (2019).

905 18. Wolfe, B. E., Button, J. E., Santarelli, M. & Dutton, R. J. Cheese Rind Communities Provide
906 Tractable Systems for In Situ and In Vitro Studies of Microbial Diversity. *Cell* **158**, 422–
907 433 (2014).

908 19. Wolfe, B. E. & Dutton, R. J. Fermented foods as experimentally tractable microbial
909 ecosystems. *Cell* **161**, 49–55 (2015).

910 20. May, A. *et al.* Kombucha: a novel model system for cooperation and conflict in a complex
911 multi-species microbial ecosystem. *PeerJ* **7**, e7565 (2019).

912 21. Morin, M., Pierce, E. C. & Dutton, R. J. Changes in the genetic requirements for microbial
913 interactions with increasing community complexity. *Elife* **7**, (2018).

914 22. Zhang, Y., Kastman, E. K., Guasto, J. S. & Wolfe, B. E. Fungal networks shape dynamics of
915 bacterial dispersal and community assembly in cheese rind microbiomes. *Nat. Commun.* **9**,
916 336 (2018).

917 23. Cleary, J. L., Kolachina, S., Wolfe, B. E. & Sanchez, L. M. Coproporphyrin III Produced by

the Bacterium Glutamicibacter arilaitensis Binds Zinc and Is Upregulated by Fungi in Cheese Rinds. *mSystems* **3**, (2018).

24. Wetmore, K. M. *et al.* Rapid Quantification of Mutant Fitness in Diverse Bacteria by Sequencing Randomly Bar-Coded Transposons. *MBio* **6**, (2015).
25. Rubin, B. E. *et al.* The essential gene set of a photosynthetic organism. *Proceedings of the National Academy of Sciences* **112**, E6634–E6643 (2015).
26. Price, M. N. *et al.* Mutant phenotypes for thousands of bacterial genes of unknown function. *Nature* **557**, 503–509 (2018).
27. Cole, B. J. *et al.* Genome-wide identification of bacterial plant colonization genes. *PLoS Biol.* **15**, e2002860 (2017).
28. Hallen-Adams, H. E. & Suhr, M. J. Fungi in the healthy human gastrointestinal tract. *Virulence* **8**, 352–358 (2017).
29. Frąc, M., Hannula, S. E., Bełka, M. & Jędryczka, M. Fungal Biodiversity and Their Role in Soil Health. *Front. Microbiol.* **9**, 707 (2018).
30. Richards, T. A., Jones, M. D. M., Leonard, G. & Bass, D. Marine fungi: their ecology and molecular diversity. *Ann. Rev. Mar. Sci.* **4**, 495–522 (2012).
31. Frey-Klett, P. *et al.* Ectomycorrhizal symbiosis affects functional diversity of rhizosphere fluorescent pseudomonads. *New Phytol.* **165**, 317–328 (2005).
32. Lopez-Medina, E. *et al.* Candida albicans Inhibits Pseudomonas aeruginosa Virulence through Suppression of Pyochelin and Pyoverdine Biosynthesis. *PLoS Pathog.* **11**, e1005129 (2015).
33. Nguyen, D. D. *et al.* Indexing the Pseudomonas specialized metabolome enabled the discovery of poaeamide B and the bananamides. *Nat Microbiol* **2**, 16197 (2016).

941 34. Choi, K.-H., Lee, H., Lee, S., Kim, S. & Yoon, Y. Cheese Microbial Risk Assessments - A
942 Review. *Asian-australas. J. Anim. Sci.* **29**, 307–314 (2016).
943 35. Perrin, F. *et al.* Quantitative Risk Assessment of Haemolytic and Uremic Syndrome Linked
944 to O157:H7 and Non-O157:H7 Shiga-Toxin Producing Escherichia coli Strains in Raw Milk
945 Soft Cheeses : Quantitative Risk Assessment of HUS Linked to Pathogenic STEC in
946 Cheese. *Risk Anal.* **35**, 109–128 (2015).
947 36. Ronquist, F. & Huelsenbeck, J. P. MrBayes 3: Bayesian phylogenetic inference under mixed
948 models. *Bioinformatics* **19**, 1572–1574 (2003).
949 37. Jukes, T. H. & Cantor, C. R. Evolution of protein molecules. *Mammalian protein*
950 *metabolism* (1969).
951 38. Cosetta, C. M. & Wolfe, B. E. Deconstructing and Reconstructing Cheese Rind
952 Microbiomes for Experiments in Microbial Ecology and Evolution. *Curr. Protoc. Microbiol.*
953 **56**, e95 (2020).
954 39. Conway, J. R., Lex, A. & Gehlenborg, N. UpSetR: an R package for the visualization of
955 intersecting sets and their properties. *Bioinformatics* **33**, 2938–2940 (2017).
956 40. Farris, C., Sanowar, S., Bader, M. W., Pfuetzner, R. & Miller, S. I. Antimicrobial peptides
957 activate the Rcs regulon through the outer membrane lipoprotein RcsF. *J. Bacteriol.* **192**,
958 4894–4903 (2010).
959 41. Laubacher, M. E. & Ades, S. E. The Rcs phosphorelay is a cell envelope stress response
960 activated by peptidoglycan stress and contributes to intrinsic antibiotic resistance. *J.*
961 *Bacteriol.* **190**, 2065–2074 (2008).
962 42. Majdalani, N., Heck, M., Stout, V. & Gottesman, S. Role of RcsF in signaling to the Rcs
963 phosphorelay pathway in Escherichia coli. *J. Bacteriol.* **187**, 6770–6778 (2005).

964 43. Yethon, J. A., Heinrichs, D. E., Monteiro, M. A., Perry, M. B. & Whitfield, C. Involvement
965 of waaY, waaQ, andwaaP in the Modification of Escherichia coliLipopolysaccharide and
966 Their Role in the Formation of a Stable Outer Membrane. *J. Biol. Chem.* **273**, 26310–26316
967 (1998).
968 44. Bociek, K. *et al.* Lipopolysaccharide Phosphorylation by the WaaY Kinase Affects the
969 Susceptibility of Escherichia coli to the Human Antimicrobial Peptide LL-37. *J. Biol. Chem.*
970 **290**, 19933–19941 (2015).
971 45. Lofton, H., Pränting, M., Thulin, E. & Andersson, D. I. Mechanisms and fitness costs of
972 resistance to antimicrobial peptides LL-37, CNY100HL and wheat germ histones. *PLoS One*
973 **8**, e68875 (2013).
974 46. Nonejuie, P., Burkart, M., Pogliano, K. & Pogliano, J. Bacterial cytological profiling rapidly
975 identifies the cellular pathways targeted by antibacterial molecules. *Proc. Natl. Acad. Sci. U.*
976 *S. A.* **110**, 16169–16174 (2013).
977 47. Laich, F., Fierro, F. & Martín, J. F. Production of penicillin by fungi growing on food
978 products: identification of a complete penicillin gene cluster in Penicillium griseofulvum
979 and a truncated cluster in Penicillium verrucosum. *Appl. Environ. Microbiol.* **68**, 1211–1219
980 (2002).
981 48. Staggs, C. G., Sealey, W. M., McCabe, B. J., Teague, A. M. & Mock, D. M. Determination
982 of the biotin content of select foods using accurate and sensitive HPLC/avidin binding. *J.*
983 *Food Compost. Anal.* **17**, 767–776 (2004).
984 49. Streit, W. R. & Entcheva, P. Biotin in microbes, the genes involved in its biosynthesis, its
985 biochemical role and perspectives for biotechnological production. *Appl. Microbiol.*
986 *Biotechnol.* **61**, 21–31 (2003).

987 50. Hall, C. & Dietrich, F. S. The reacquisition of biotin prototrophy in Saccharomyces
988 cerevisiae involved horizontal gene transfer, gene duplication and gene clustering. *Genetics*
989 **177**, 2293–2307 (2007).
990 51. Bonham, K. S., Wolfe, B. E. & Dutton, R. J. Extensive horizontal gene transfer in cheese-
991 associated bacteria. *Elife* **6**, (2017).
992 52. Kastman, E. K. *et al.* Biotic Interactions Shape the Ecological Distributions of
993 Staphylococcus Species. *MBio* **7**, (2016).
994 53. Monnet, C., Back, A. & Irlinger, F. Growth of aerobic ripening bacteria at the cheese
995 surface is limited by the availability of iron. *Appl. Environ. Microbiol.* **78**, 3185–3192
996 (2012).
997 54. Blin, K. *et al.* antiSMASH 5.0: updates to the secondary metabolite genome mining
998 pipeline. *Nucleic Acids Res.* **47**, W81–W87 (2019).
999 55. Hantke, K. Identification of an iron uptake system specific for coprogen and rhodotorulic
1000 acid in Escherichia coli K12. *Mol. Gen. Genet.* **191**, 301–306 (1983).
1001 56. Fecker, L. & Braun, V. Cloning and expression of the fhu genes involved in iron(III)-
1002 hydroxamate uptake by Escherichia coli. *J. Bacteriol.* **156**, 1301–1314 (1983).
1003 57. Sauer, M., Hantke, K. & Braun, V. Ferric-coprogen receptor FhuE of Escherichia coli:
1004 processing and sequence common to all TonB-dependent outer membrane receptor proteins.
1005 *J. Bacteriol.* **169**, 2044–2049 (1987).
1006 58. Matzanke, B. F., Anemüller, S., Schünemann, V., Trautwein, A. X. & Hantke, K. FhuF, part
1007 of a siderophore-reductase system. *Biochemistry* **43**, 1386–1392 (2004).
1008 59. Pain, A. *et al.* Insight into the genome of Aspergillus fumigatus: analysis of a 922kb region
1009 encompassing the nitrate assimilation gene cluster. *Fungal Genet. Biol.* **41**, 443–453 (2004).

1010 60. Chryssanthou, E., Broberger, U. & Petrini, B. Malassezia pachydermatis fungaemia in a
1011 neonatal intensive care unit. *Acta Paediatr.* **90**, 323–327 (2007).
1012 61. Prohic, A., Jovovic Sadikovic, T., Krupalija-Fazlic, M. & Kuskunovic-Vlahovljak, S.
1013 Malassezia species in healthy skin and in dermatological conditions. *Int. J. Dermatol.* **55**,
1014 494–504 (2016).
1015 62. Haas, H. Fungal siderophore metabolism with a focus on Aspergillus fumigatus. *Nat. Prod.*
1016 *Rep.* **31**, 1266–1276 (2014).
1017 63. Park, M., Cho, Y.-J., Lee, Y. W. & Jung, W. H. Understanding the Mechanism of Action of
1018 the Anti-Dandruff Agent Zinc Pyrithione against Malassezia restricta. *Sci. Rep.* **8**, 12086
1019 (2018).
1020 64. Gründlinger, M. *et al.* Fungal siderophore biosynthesis is partially localized in peroxisomes.
1021 *Mol. Microbiol.* **88**, 862–875 (2013).
1022 65. Wu, G. *et al.* Genus-Wide Comparative Genomics of Malassezia Delineates Its Phylogeny,
1023 Physiology, and Niche Adaptation on Human Skin. *PLoS Genet.* **11**, e1005614 (2015).
1024 66. Triana, S. *et al.* Draft Genome Sequence of the Animal and Human Pathogen Malassezia
1025 pachydermatis Strain CBS 1879. *Genome Announc.* **3**, (2015).
1026 67. Perrin, R. M. *et al.* Transcriptional regulation of chemical diversity in Aspergillus fumigatus
1027 by LaeA. *PLoS Pathog.* **3**, e50 (2007).
1028 68. Bok, J. W. & Keller, N. P. LaeA, a regulator of secondary metabolism in Aspergillus spp.
1029 *Eukaryot. Cell* **3**, 527–535 (2004).
1030 69. Kosalková, K. *et al.* The global regulator LaeA controls penicillin biosynthesis,
1031 pigmentation and sporulation, but not roquefortine C synthesis in Penicillium chrysogenum.
1032 *Biochimie* **91**, 214–225 (2009).

1033 70. Bräse, S., Encinas, A., Keck, J. & Nising, C. F. Chemistry and biology of mycotoxins and
1034 related fungal metabolites. *Chem. Rev.* **109**, 3903–3990 (2009).
1035 71. Luckner, M. [On the synthesis of quinoline alkaloids in plants. 2. Fermentative conversion
1036 of the penicillin alkaloids cyclopenin and cyclopenol to viridicatin and viridicatol]. *Eur. J.*
1037 *Biochem.* **2**, 74–78 (1967).
1038 72. Ma, Y.-M. *et al.* A new isoquinolone alkaloid from an endophytic fungus R22 of Nerium
1039 indicum. *Nat. Prod. Res.* **31**, 951–958 (2017).
1040 73. Dalsgaard, P. W. *et al.* Atlantinone A, a Meroterpenoid Produced by Penicillium ribeum and
1041 Several Cheese Associated Penicillium Species. *Metabolites* **2**, 214–220 (2012).
1042 74. Wang, X. *et al.* Chemical epigenetics alters the secondary metabolite composition of guttate
1043 excreted by an atlantic-forest-soil-derived Penicillium citreonigrum. *J. Nat. Prod.* **73**, 942–
1044 948 (2010).
1045 75. Tomoda, H. *et al.* Pyripyropenes, novel ACAT inhibitors produced by Aspergillus
1046 fumigatus. IV. Structure elucidation of pyripyropenes M to R. *J. Antibiot.* **49**, 292–298
1047 (1996).
1048 76. Patti, G. J. *et al.* A view from above: cloud plots to visualize global metabolomic data. *Anal.*
1049 *Chem.* **85**, 798–804 (2013).
1050 77. Peters, B. M., Jabra-Rizk, M. A., O'May, G. A., Costerton, J. W. & Shirtliff, M. E.
1051 Polymicrobial interactions: impact on pathogenesis and human disease. *Clin. Microbiol.*
1052 *Rev.* **25**, 193–213 (2012).
1053 78. Shirtliff, M. E., Peters, B. M. & Jabra-Rizk, M. A. Cross-kingdom interactions: Candida
1054 albicans and bacteria. *FEMS Microbiol. Lett.* **299**, 1–8 (2009).
1055 79. Scherlach, K., Graupner, K. & Hertweck, C. Molecular bacteria-fungi interactions: effects

1056 on environment, food, and medicine. *Annu. Rev. Microbiol.* **67**, 375–397 (2013).
1057 80. Wargo, M. J. & Hogan, D. A. Fungal—bacterial interactions: a mixed bag of mingling
1058 microbes. *Curr. Opin. Microbiol.* **9**, 359–364 (2006/8).
1059 81. Leclair, L. W. & Hogan, D. A. Mixed bacterial-fungal infections in the CF respiratory tract.
1060 *Med. Mycol.* **48 Suppl 1**, S125–32 (2010).
1061 82. Kim, D. *et al.* Candida albicans stimulates Streptococcus mutans microcolony development
1062 via cross-kingdom biofilm-derived metabolites. *Sci. Rep.* **7**, 41332 (2017).
1063 83. de Boer, W. & Folman, L. B. Living in a fungal world: impact of fungi on soil bacterial
1064 niche development. *FEMS microbiology* (2005).
1065 84. Johansson, J. F., Paul, L. R. & Finlay, R. D. Microbial interactions in the mycorrhizosphere
1066 and their significance for sustainable agriculture. *FEMS Microbiol. Ecol.* **48**, 1–13 (2004).
1067 85. Tarkka, M. T., Sarniguet, A. & Frey-Klett, P. Inter-kingdom encounters: recent advances in
1068 molecular bacterium-fungus interactions. *Curr. Genet.* **55**, 233–243 (2009).
1069 86. Moree, W. J. *et al.* Interkingdom metabolic transformations captured by microbial imaging
1070 mass spectrometry. *Proc. Natl. Acad. Sci. U. S. A.* **109**, 13811–13816 (2012).
1071 87. Clancy, A. *et al.* Evidence for siderophore-dependent iron acquisition in group B
1072 streptococcus. *Mol. Microbiol.* **59**, 707–721 (2006).
1073 88. Jin, B. *et al.* Iron acquisition systems for ferric hydroxamates, haemin and haemoglobin in
1074 Listeria monocytogenes. *Mol. Microbiol.* **59**, 1185–1198 (2006).
1075 89. Sheldon, J. R. & Heinrichs, D. E. Recent developments in understanding the iron acquisition
1076 strategies of gram positive pathogens. *FEMS Microbiol. Rev.* **39**, 592–630 (2015).
1077 90. Arias, A. A. *et al.* Growth of desferrioxamine-deficient Streptomyces mutants through
1078 xenosiderophore piracy of airborne fungal contaminations. *FEMS Microbiol. Ecol.* **91**,

1079 (2015).
1080 91. Mishra, R. P. N. *et al.* Staphylococcus aureus FhuD2 is involved in the early phase of
1081 staphylococcal dissemination and generates protective immunity in mice. *J. Infect. Dis.* **206**,
1082 1041–1049 (2012).
1083 92. Li, H. *et al.* The outer mucus layer hosts a distinct intestinal microbial niche. *Nat. Commun.*
1084 **6**, 8292 (2015).
1085 93. Rocha, E. R. & Krykunivsky, A. S. Anaerobic utilization of Fe(III)-xenosiderophores
1086 among Bacteroides species and the distinct assimilation of Fe(III)-ferrichrome by
1087 Bacteroides fragilis within the genus. *Microbiologyopen* **6**, (2017).
1088 94. Emri, T. *et al.* Towards high-siderophore-content foods: optimisation of coprogen
1089 production in submerged cultures of Penicillium nalgiovense. *J. Sci. Food Agric.* **93**, 2221–
1090 2228 (2013).
1091 95. Ong, S. A. & Neilands, J. B. Siderophores in microbially processed cheese. *J. Agric. Food*
1092 *Chem.* **27**, 990–995 (1979).
1093 96. David, L. A. *et al.* Diet rapidly and reproducibly alters the human gut microbiome. *Nature*
1094 **505**, 559–563 (2014).
1095 97. Rehner, S. A. & Samuels, G. J. Molecular systematics of the Hypocreales: a teleomorph
1096 gene phylogeny and the status of their anamorphs. *Can. J. Bot.* **73**, 816–823 (1995).
1097 98. Glass, N. L. & Donaldson, G. C. Development of primer sets designed for use with the PCR
1098 to amplify conserved genes from filamentous ascomycetes. *Appl. Environ. Microbiol.* **61**,
1099 1323–1330 (1995).
1100 99. Dunnett, C. W. A Multiple Comparison Procedure for Comparing Several Treatments with a
1101 Control. *J. Am. Stat. Assoc.* **50**, 1096–1121 (1955).

1102 100. Wickham, H. ggplot2: Elegant Graphics for Data Analysis. (2009).
1103 101. Cleary, J. L., Luu, G. T., Pierce, E. C., Dutton, R. J. & Sanchez, L. M. BLANKA: an
1104 Algorithm for Blank Subtraction in Mass Spectrometry of Complex Biological Samples. *J.*
1105 *Am. Soc. Mass Spectrom.* **30**, 1426–1434 (2019).
1106 102. Mohimani, H. *et al.* Dereplication of microbial metabolites through database search of mass
1107 spectra. *Nature Communications* vol. 9 (2018).
1108 103. Mohimani, H. *et al.* Dereplication of peptidic natural products through database search of
1109 mass spectra. *Nat. Chem. Biol.* **13**, 30–37 (2017).
1110 104. Shannon, P. *et al.* Cytoscape: a software environment for integrated models of biomolecular
1111 interaction networks. *Genome Res.* **13**, 2498–2504 (2003).
1112 105. Tang, Y., Horikoshi, M. & Li, W. ggfortify: Unified Interface to Visualize Statistical Result
1113 of Popular R Packages. *The R Journal* vol. 8 (2016).
1114 106. Huerta-Cepas, J. *et al.* eggNOG 5.0: a hierarchical, functionally and phylogenetically
1115 annotated orthology resource based on 5090 organisms and 2502 viruses. *Nucleic Acids Res.*
1116 **47**, D309–D314 (2019).
1117 107. Baba, T. *et al.* Construction of Escherichia coli K-12 in-frame, single-gene knockout
1118 mutants: the Keio collection. *Mol. Syst. Biol.* **2**, 2006.0008 (2006).
1119 108. Schindelin, J. *et al.* Fiji: an open-source platform for biological-image analysis. *Nat.*
1120 *Methods* **9**, 676–682 (2012).
1121 109. Grenier, F., Matteau, D., Baby, V. & Rodrigue, S. Complete Genome Sequence of
1122 Escherichia coli BW25113. *Genome Announc.* **2**, (2014).
1123 110. Lawrence, M. *et al.* Software for computing and annotating genomic ranges. *PLoS Comput.*
1124 *Biol.* **9**, e1003118 (2013).

1125 111. Love, M. I., Huber, W. & Anders, S. Moderated estimation of fold change and dispersion
1126 for RNA-seq data with DESeq2. *Genome Biol.* **15**, 550 (2014).
1127 112. Datsenko, K. A. & Wanner, B. L. One-step inactivation of chromosomal genes in
1128 Escherichia coli K-12 using PCR products. *Proc. Natl. Acad. Sci. U. S. A.* **97**, 6640–6645
1129 (2000).
1130 113. Koren, S. *et al.* Canu: scalable and accurate long-read assembly via adaptive k-mer
1131 weighting and repeat separation. *Genome Res.* **27**, 722–736 (2017).
1132 114. Vaser, R., Sović, I., Nagarajan, N. & Šikić, M. Fast and accurate de novo genome assembly
1133 from long uncorrected reads. *Genome Res.* **27**, 737–746 (2017).
1134 115. Walker, B. J. *et al.* Pilon: an integrated tool for comprehensive microbial variant detection
1135 and genome assembly improvement. *PLoS One* **9**, e112963 (2014).
1136 116. Min, B., Grigoriev, I. V. & Choi, I.-G. FunGAP: Fungal Genome Annotation Pipeline using
1137 evidence-based gene model evaluation. *Bioinformatics* **33**, 2936–2937 (2017).
1138 117. Jones, P. *et al.* InterProScan 5: genome-scale protein function classification. *Bioinformatics*
1139 **30**, 1236–1240 (2014).
1140 118. Lim, F. Y., Sanchez, J. F., Wang, C. C. C. & Keller, N. P. Toward awakening cryptic
1141 secondary metabolite gene clusters in filamentous fungi. *Methods Enzymol.* **517**, 303–324
1142 (2012).
1143 119. Xie, C. *et al.* KOBAS 2.0: a web server for annotation and identification of enriched
1144 pathways and diseases. *Nucleic Acids Res.* **39**, W316–22 (2011).
1145 120. The Gene Ontology Consortium. The Gene Ontology Resource: 20 years and still GOing
1146 strong. *Nucleic Acids Res.* **47**, D330–D338 (2019).
1147 121. Ashburner, M. *et al.* Gene ontology: tool for the unification of biology. The Gene Ontology

Consortium. *Nat. Genet.* **25**, 25–29 (2000).

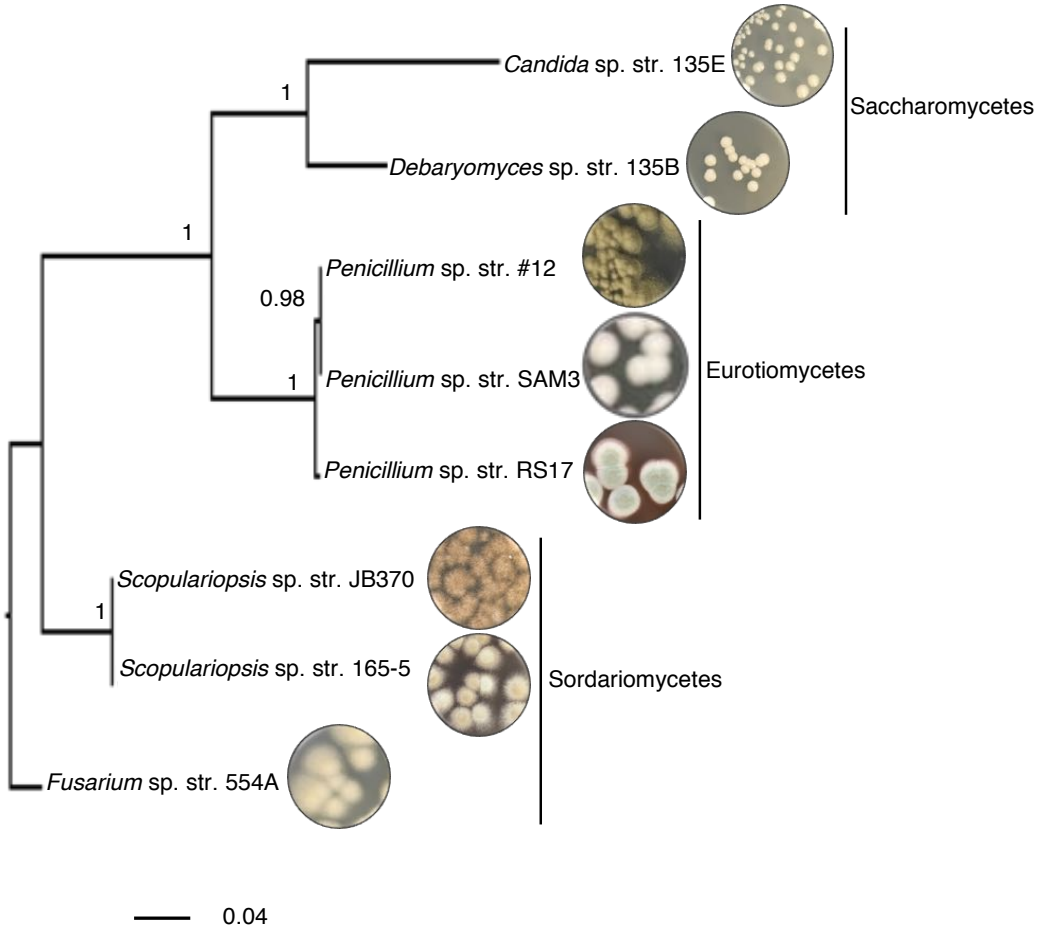

1178
1179
1180
1181 **Figure 1: Fungal interaction partners span the phylogenetic and morphological diversity of**
1182 **the cheese ecosystem.** Phylogenetic tree based on large subunit rRNA of the cheese fungi used
1183 as interaction partners in this study. The tree was built using Bayesian phylogenetic inference
1184 with MrBayes[36] and the Jukes and Cantor substitution model[37]. Branch labels display posterior
1185 probability.
1186
1187
1188
1189
1190
1191
1192
1193
1194
1195

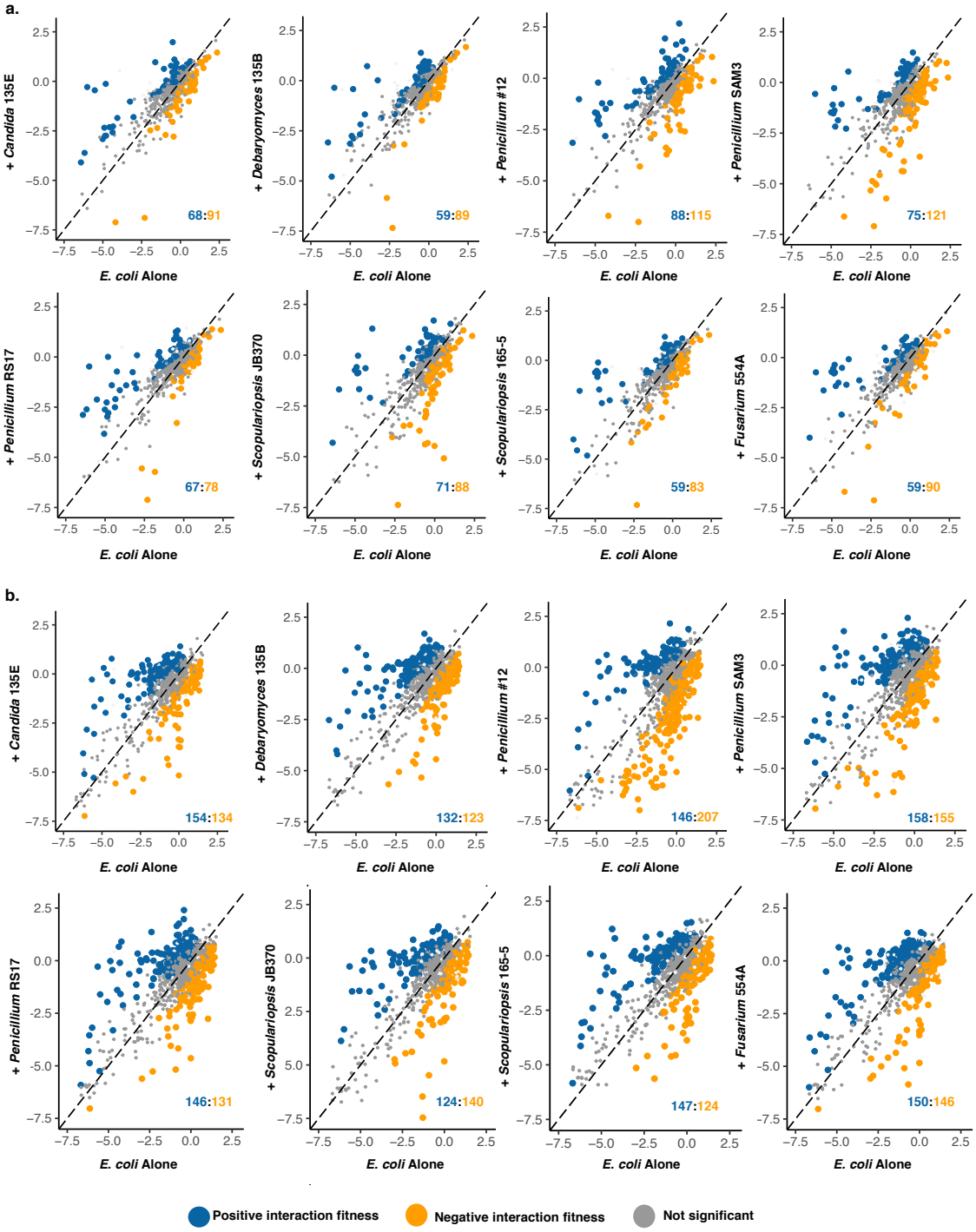

Figure 2: Bacterial genes with significant interaction fitness across fungal partners. Each dot represents a gene, with colored dots indicating genes with a significant interaction fitness. X and Y values indicate gene fitness values in each condition (alone on x-axis versus grown with a fungal partner on y-axis), and the colored numbers in the lower right hand corner indicate how

many genes have either positive (blue) or negative (orange) interaction fitness. **a,** *E. coli.* **b,** *P. psychrophila.*

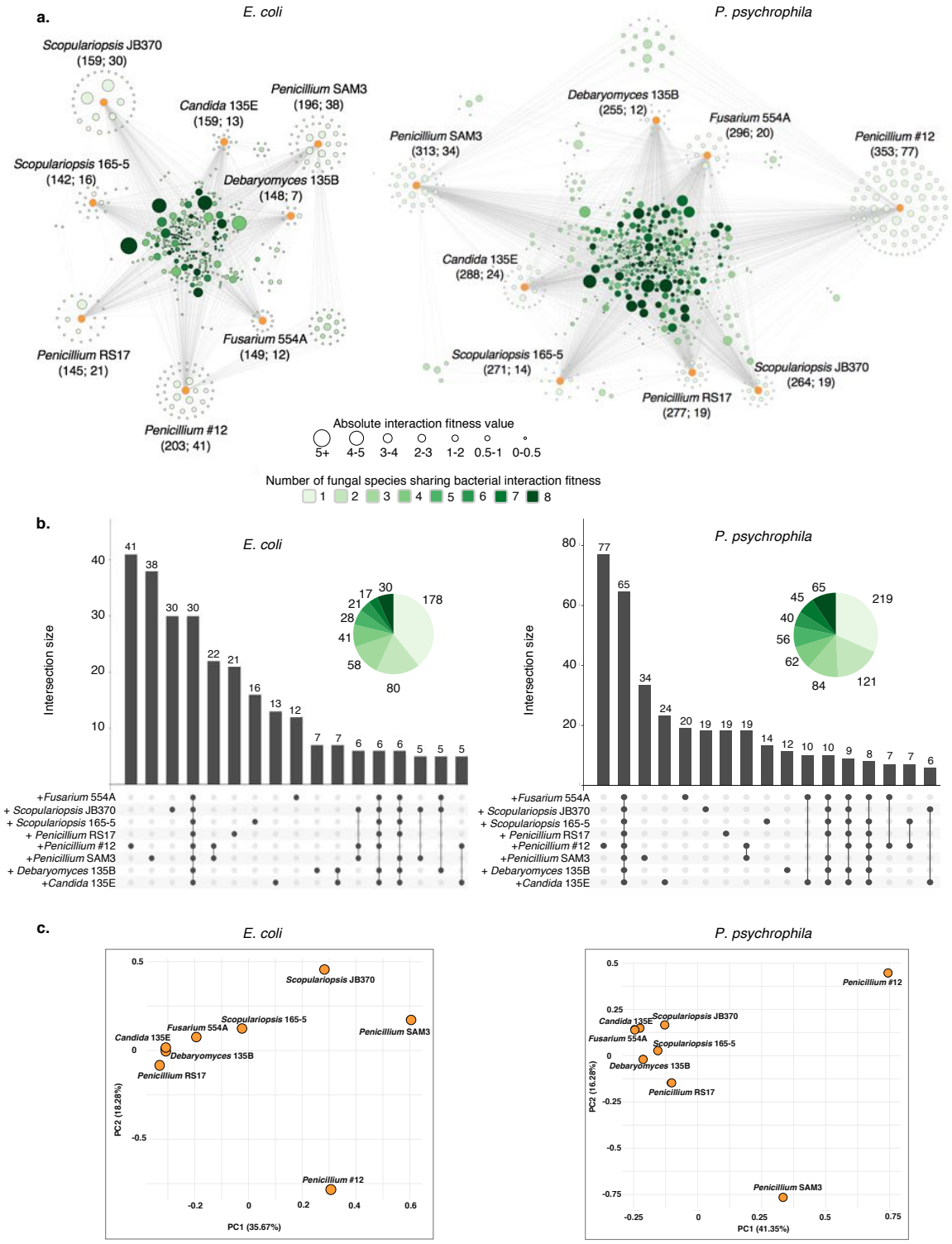

Figure 3: Bacterial genes with differential fitness in the presence of fungi. **a,** Network of *E. coli* (left) or *P. psychrophila* (right) genes with an interaction fitness based on RB-TnSeq. Each orange node represents a fungal partner and is labeled as follows: Fungal partner (Number of genes with interaction fitness; Number of genes with interaction fitness unique to this condition). Each green node represents a bacterial gene. They are colored by the number of fungal conditions in which this gene has an interaction fitness as shown in the legend below. They are sized by average strength of interaction fitness across partners. **b,** UpSet[39] plots showing the overlaps, or intersections, of *E. coli* (left) or *P. psychrophila* (right) gene sets with interaction fitness across fungal partners. These UpSet plots are conceptually similar to Venn Diagrams. The connected circles indicate which fungal conditions are included in the intersection, and the size of the intersection (the number of genes that have an interaction fitness in all the highlighted conditions) is displayed in the main bar chart. Intersections <5 genes are not shown. For example, in the *E. coli* panel, 30 genes have an interaction fitness with all partners (all fungi circles are connected), while 22 other genes have an interaction fitness with *Penicillium* sp. str. #12 and with *Penicillium* sp. str. SAM3 (only *Penicillium* sp. str. #12 *and Penicillium* sp. str. SAM3 circles are connected). **c,** PCA of the raw fitness values for all *E. coli* (left) or *P. psychrophila* (right) genes with an interaction fitness in at least one fungal condition.

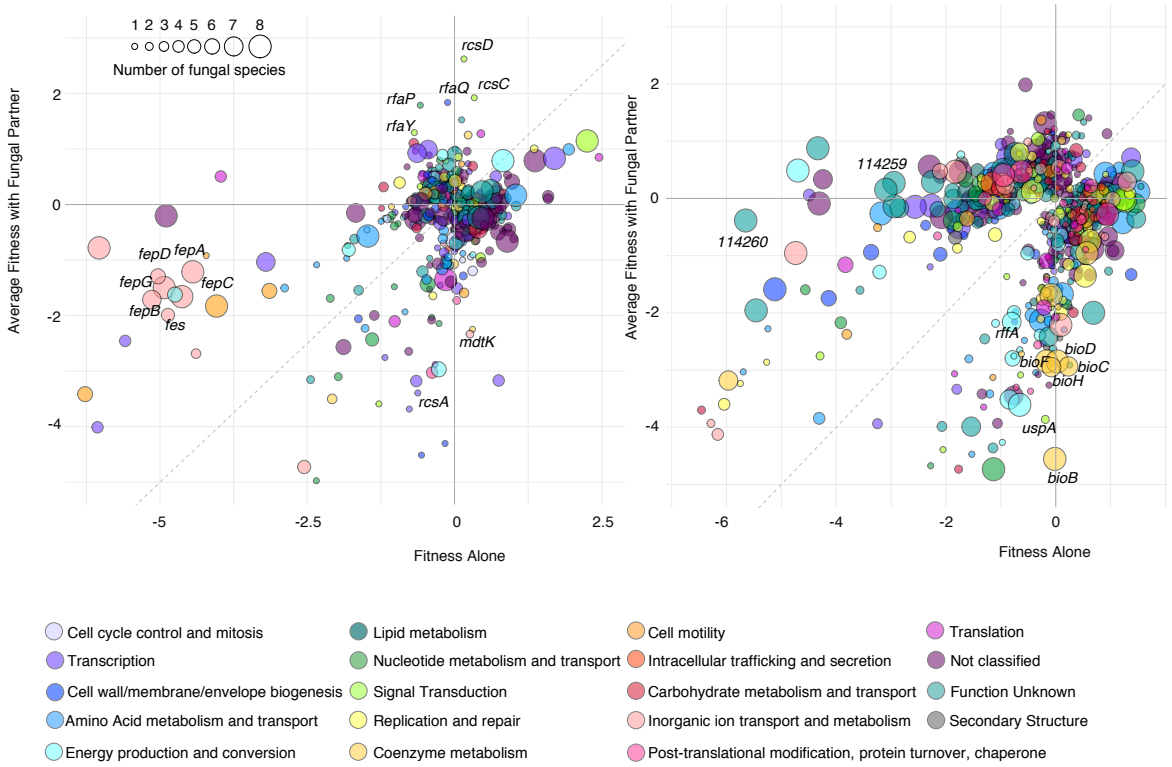

Figure 4: Functional analysis of the bacterial genes associated with interaction fitness. Comparison of *E. coli* (left) or *P. psychrophila* (right) gene fitness values alone compared to fitness values with a fungal partner, colored by COG category and sized by the conservation of effect among fungal partners (1-8 fungal species).

1274

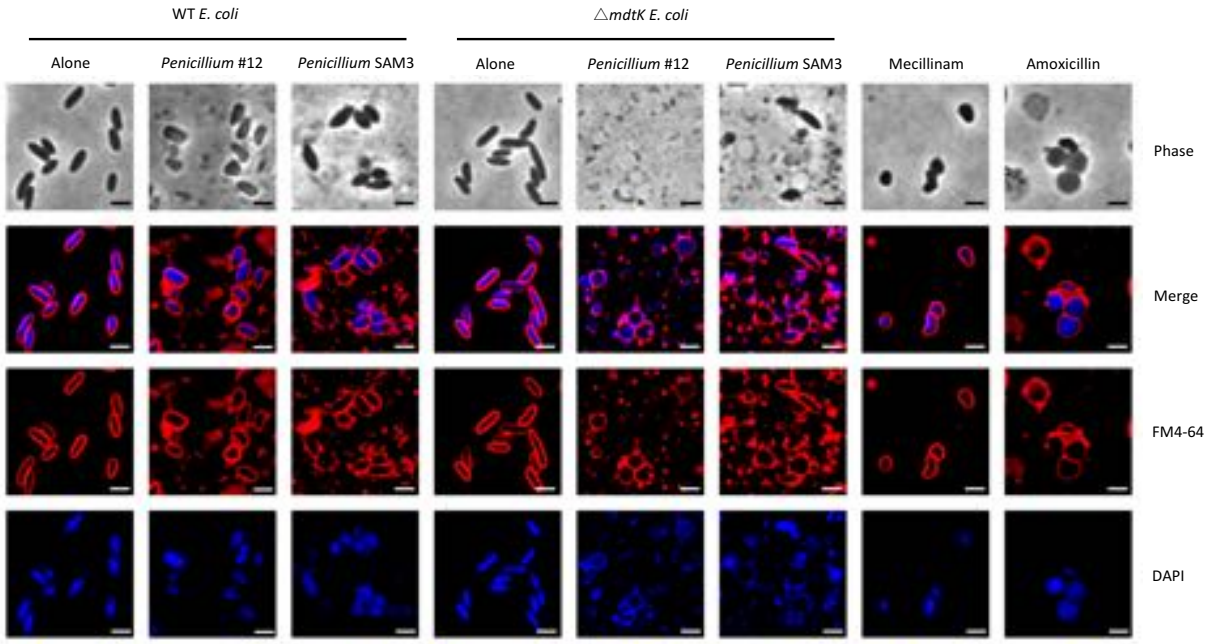

1275
1276
1277 **Figure 5: Bacterial cytological profiling of *E. coli* grown in a mixed biofilm with *Penicillium***
1278 **sp. str. #12 and *Penicillium* sp. str. SAM3 on CCA plates.** The phenotype of *E. coli* grown
1279 with these fungi is similar to that seen when *E. coli* is exposed to antibiotics targeting cell wall
1280 biosynthesis. DAPI dye stains DNA and FM4-64 dye stains bacterial membranes. Scale bars
1281 represent 2 μm.
1282
1283
1284
1285
1286
1287
1288
1289
1290
1291
1292
1293
1294
1295
1296
1297
1298
1299
1300

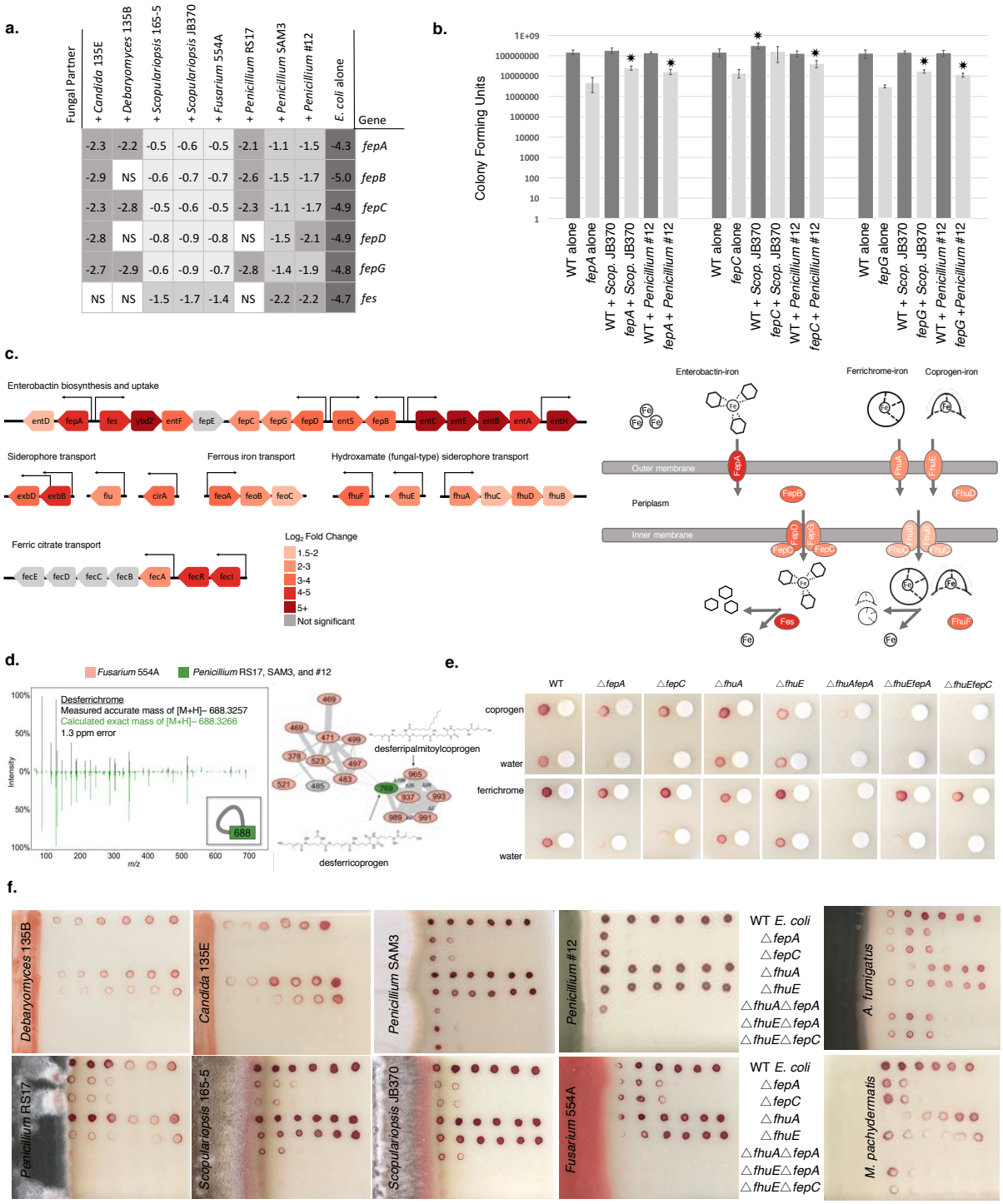

Figure 6: Utilization of fungal siderophores by *E. coli*. a, RB-TnSeq fitness values for *fep* operon genes in alone or interactive conditions, showing an increase in fitness in the presence of fungal species. NS- not significant. **b,** Colony forming units of WT and Δ*fep* mutants after 7 days of 1:1 competitive growth on CCA. Competitions were performed either alone or with

1307 *Penicillium* sp. str. #12 or *Scopulariopsis* sp. str. JB370. Asterisk indicates significantly different
1308 growth in the presence of a fungus relative to growth alone (t-test p-value < 0.05). **c,** *E. coli* iron-
1309 related genes upregulated in the presence of *Penicillium* sp. str. #12. Significance cutoff made at
1310 abs($\log_2$(fold-change)) >1.5 and adjusted p-value <0.05. **d,** Fungal siderophores identified by
1311 mass spectrometry. Insets show the node that represents the desferrichrome fragmentation
1312 pattern depicted. Coprogen B and ferrichrome were found by matching fragmentation patterns to
1313 library spectra. Both identifications were confirmed using retention time and fragmentation
1314 matching to a purchased standard. **e,** Visual assays of *Δfep* mutant growth with purified
1315 siderophores coprogen and ferrichrome. **f,** Visual assays of *E. coli* mutant growth at varying
1316 distances from cheese fungi, *A. fumigatus* (soil, human pathogen), and *M. pachydermatis* (skin
1317 commensal).
1318
1319
1320
1321
1322
1323
1324
1325
1326
1327
1328
1329
1330
1331
1332
1333
1334
1335
1336
1337
1338
1339
1340
1341
1342
1343
1344
1345
1346
1347
1348
1349
1350
1351
1352

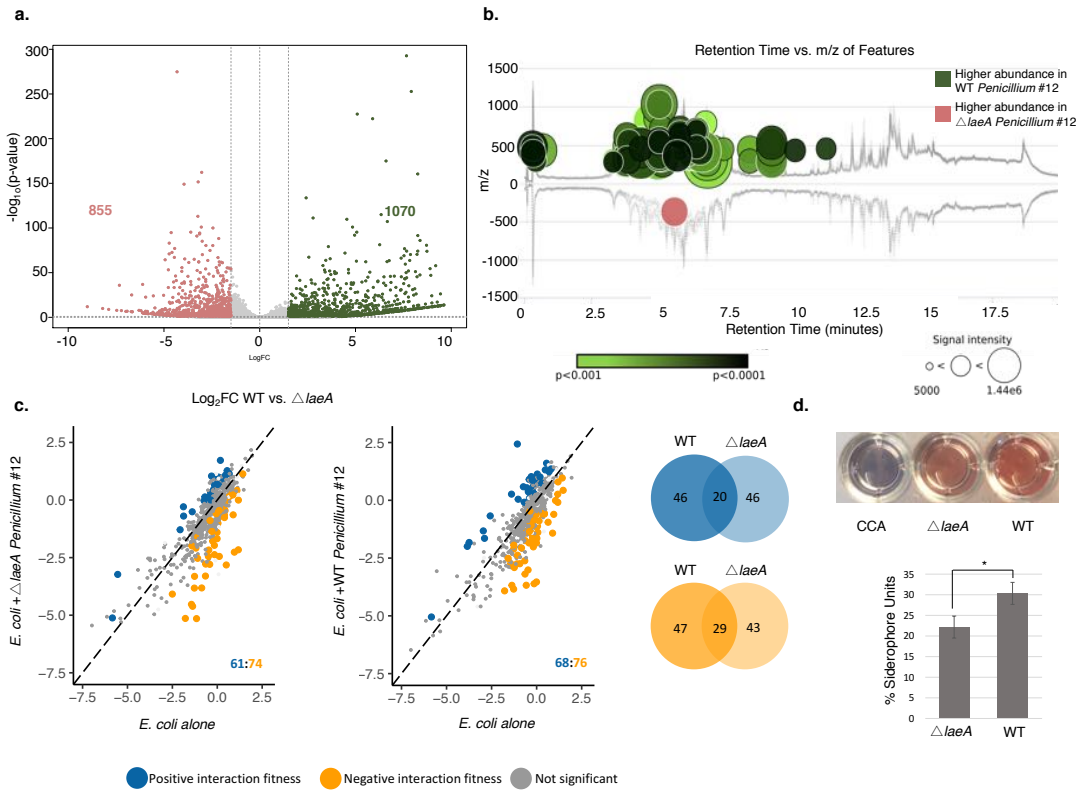

Figure 7: Fungal metabolite production impacts bacterial-fungal interactions. a, Differential expression of WT *Penicillium* sp. str. #12 relative to Δ*laeA* after three days of growth on CCA. Labeled on the volcano plot are the number of genes with a $\log_2$FC of >1.5 (green) or <-1.5 (red) and adjusted p-value of <0.05. **b,** The metabolomics data analysis platform XCMS[76] was used to compare features detected by LC-MS analyses of Δ*laeA* and WT *Penicillium* sp. str. #12 extracts. Features of higher abundance in WT relative to Δ*laeA* are depicted as green nodes on the top of the mirror plot and features of lower abundance in WT relative to Δ*laeA* are depicted as red nodes on the bottom. Node radius is proportional to the fold change of the detected features and color intensity is dependent on p-value. The graph displays only those features with a p value less than or equal to 0.05, fold change higher than or equal to 10, *m/z* between 200 and 2000 Da, and intensity higher than 500. **c,** *E. coli* genes with significant interaction fitness with Δ*laeA* and WT *Penicillium* sp. str. #12. Each dot represents a gene, with colored dots indicating genes with interaction fitness. X and Y values (alone on x-axis and +fungal partner on y-axis) indicate gene fitness values in each condition, and the numbers in the lower right hand corner indicate how many genes have either positive (blue) or negative (orange) interaction fitness. Venn diagrams display the overlap of these gene sets. **d,** Liquid CAS assay of supernatants from blank control CCA medium, Δ*laeA,* or WT *Penicillium* sp. str. #12. Asterisk indicates significantly different siderophore production (t-test p-value < 0.05).

1372 **SUPPLEMENTAL FIGURE AND TABLE LEGENDS**
1373
1374 **Supplementary Figure 1**: **Impacts of fungal species on bacterial growth after 7 days of coculture on**
1375 **cheese curd agar, pH 7**. CFU: colony forming units. * represents a significant difference in bacterial
1376 growth in the presence of the fungal partner relative to alone (Dunnett's test, p-value <.05).
1377
1378 **Supplementary Figure 2**: **Impacts of bacterial species on fungal growth after 7 days of coculture on**
1379 **cheese curd agar, pH 7**. Spore counts were used as a proxy for fungal growth. * represents a significant
1380 difference in fungal growth in the presence of the bacterial partner relative to alone (Dunnett's test, p-
1381 value <.05).
1382
1383 **Supplementary Figure 3: RB-TnSeq assay workflow.** Characterized pooled bacterial mutant libraries
1384 were grown in a biofilm either alone or in a mixed biofilm with a fungal partner. After seven days of
1385 growth, mutant abundances were compared to the starting library abundances for each condition.
1386 Changes in barcode abundances were used to calculate gene fitness values. Genes with fitness values that
1387 differed significantly between co-culture and alone conditions (significant interaction fitness) were
1388 identified as potentially relevant to fungal interaction.
1389
1390 **Supplementary Figure 4: COG categories of genes with interaction fitness.** Number of genes with
1391 interaction fitness falling into each COG category for *E. coli* (left) or *P. psychrophila* (right).
1392
1393 **Supplementary Figure 5: Bacterial Cytological Profiling of △*tolC E.coli* treated with known**
1394 **antibiotic compounds on cheese curd agar.** DAPI dye stains DNA and FM4-64 dye stains bacterial
1395 membranes. SYTOX green stains nucleic acids but cannot penetrate live cells.
1396
1397 **Supplementary Figure 6**: **Siderophore production by filamentous molds.** Liquid CAS assay was
1398 performed on filtered and concentrated fungal supernatants from three replicates grown in liquid cheese
1399 for 12 days. Row A) 1-3: Liquid cheese control 4-6: *Penicillium* SAM3. Row B) 1-3: *Debaryomyces*
1400 135B 4-6: *Penicillium* #12. Row C) 1-3: *Candida* 135E. 4-6: *Penicillium* RS17. Row D) 1-3:
1401 *Scopulariopsis* 165-5 Row E) 1-3: *Scopulariopsis* JB370. Row F) 1-3: *Fusarium* 554A. % Siderophore
1402 units calculated as $[(A_r - A_s)/(A_r)]*100$, where A_r is the absorbance of the cheese curd agar supernatant
1403 blank and A_s is the absorbance of the sample. N=3, error bars show standard deviation.
1404
1405 **Supplementary Figure 7**: **Fitness defect of *fep* mutants on iron-limiting CCA.** Visual assays of *E. coli*
1406 mutant growth spotted alone on CCA pH 7.
1407
1408 **Supplementary Figure 8. Deletion of *laeA* gene in *Penicillium* sp. str. #12**. A. Schematic
1409 representation of the genetic construct for *laeA* deletion in *P. solitum* strain 12. The construct is
1410 constituted of the *hph* gene conferring resistance to hygromycin. The positions of the restriction enzyme
1411 cutting sites are shown on the map B. Southern blot analyses of genomic DNA from the WT and the
1412 Δ*laeA* strains. Ten micrograms of total DNA from each strain was digested with the appropriate enzymes
1413 and subjected to southern blot analysis using respectively the 5' flank fragment (blue) and the 3'fragment
1414 (grey) as probes. The 1 kb DNA ladder from New England Biolabs was used to determine the size of the
1415 expected bands.
1416
1417 **Supplementary Data 1: RB-TnSeq fitness values for *E. coli* grown with fungal partners compared**

to alone.

Supplementary Data 2: RB-TnSeq fitness values for *P. psychrophila* grown with fungal partners compared to alone.

Supplementary Data 3: Genes with significant interaction fitness for *E. coli* grown with fungal partners compared to alone.

Supplementary Data 4: Genes with significant interaction fitness for *P. psychrophila* grown with fungal partners compared to alone.

Supplementary Data 5: Intersection lists for *E. coli* genes with interaction fitness across all conditions.

Supplementary Data 6: Intersection lists for *P. psychrophila* genes with interaction fitness across all conditions.

Supplementary Data 7: Functional enrichment results for *E. coli* genes with interaction fitness across all conditions.

Supplementary Data 8: Functional enrichment results for *P. psychrophila* genes with interaction fitness across all conditions.

Supplementary Data 9: RNA-Seq differential expression analysis for *E. coli* grown with *Penicillium* sp. str. #12 (*E. coli* perspective, alone condition as reference).

Supplementary Data 10: Iron-related genes that are differentially expressed by *E. coli* when grown with *Penicillium* sp. str. #12 relative to *E. coli* growth alone.

Supplementary Data 11: Metabolite production by Δ*laeA* and WT *Penicillium* sp. str. #12. Δ*laeA* used as the reference condition.

Supplementary Data 12: RB-TnSeq fitness values for *E. coli* grown with Δ*laeA* or WT *Penicillium* sp. str. #12 compared to alone.

Supplementary Data 13: RNA-Seq differential expression analysis for Δ*laeA* vs. WT *Penicillium* sp. str. (WT used as the reference condition).

Supplementary Data 14: Functional enrichment results for genes differentially expressed in Δ*laeA* vs. WT *Penicillium* #12.

Supplementary Data 15: Overlap of *E. coli* or *P. psychrophila* genes with interaction fitness.

1466
1467